



Deposited via The University of Leeds.

White Rose Research Online URL for this paper:

<https://eprints.whiterose.ac.uk/id/eprint/167733/>

Version: Accepted Version

Article:

Levine, RC, Klingaman, NP, Peatman, SC et al. (2021) Roles of air-sea coupling and horizontal resolution in the climate model simulation of Indian monsoon low pressure systems. *Climate Dynamics*, 56. pp. 1203-1226. ISSN: 0930-7575

<https://doi.org/10.1007/s00382-020-05526-6>

© Crown 2020. This is an author produced version of a journal article published in *Climate Dynamics*. Uploaded in accordance with the publisher's self-archiving policy.

Reuse

Items deposited in White Rose Research Online are protected by copyright, with all rights reserved unless indicated otherwise. They may be downloaded and/or printed for private study, or other acts as permitted by national copyright laws. The publisher or other rights holders may allow further reproduction and re-use of the full text version. This is indicated by the licence information on the White Rose Research Online record for the item.

Takedown

If you consider content in White Rose Research Online to be in breach of UK law, please notify us by emailing eprints@whiterose.ac.uk including the URL of the record and the reason for the withdrawal request.

Roles of air-sea coupling and horizontal resolution in the climate model simulation of Indian monsoon low pressure systems

Richard C. Levine · Nicholas P. Klingaman · Simon C. Peatman · Gill M. Martin

the date of receipt and acceptance should be inserted later

1 Received: date / Accepted: date

2 **Abstract** The roles of air-sea coupling and horizontal
3 resolution in the representation of Indian monsoon low
4 pressure systems (LPS) in Met Office Unified Model
5 (MetUM) global climate simulations are investigated.
6 To avoid the generally large sea surface temperature
7 (SST) biases in standard coupled atmosphere-ocean global
8 climate models (GCMs), the analysis is performed on
9 experiments from an atmosphere model coupled to a
10 mixed-layer ocean model (MetUM-GOML2), which al-
11 lows coupling to be applied regionally as well as glob-
12 ally, while constraining the ocean mean state in coupled
13 regions. Compared to the standard AMIP-style MetUM
14 atmosphere-only simulations, the MetUM-GOML2 sim-
15 ulations produce more monsoon LPS, which is attributed
16 to effects of relatively small remaining (Indian Ocean)
17 SST biases that somewhat strengthen the atmospheric
18 monsoon base state. However, the MetUM-GOML2 sim-
19 ulations, all starting from the same atmospheric and
20 oceanic base state, allow for an idealised approach to
21 evaluate the relative effects of coupling and resolution.
22 When the effects of SST biases are excluded, global
23 coupling has a neutral impact on the number of LPS
24 formed, while the associated rainfall is somewhat re-
25 duced due to a local negative air-sea feedback reducing
26 the strength of atmospheric convection and weakening
27 individual LPS. The MetUM-GOML2 simulations show
28 particular sensitivity to localised coupling in the In-

dian and Pacific Oceans, which appears to enhance the
29 effect of monsoon LPS. Although, in contrast to the
30 global coupling comparison, the comparison of region-
31 ally coupled simulations is affected by both differences
32 in interannual SST variability and SST biases, and it
33 is likely that this causes at least part of the positive
34 effects from Indian and Pacific Ocean coupling. More
35 importantly, however, is that the effects of air-sea cou-
36 pling are substantially smaller than the positive effects
37 of the increase in horizontal resolution from N96 (ap-
38 prox. 200km) to N216 (approx. 90km). The resolution
39 effect is also larger than that seen in older MetUM con-
40 figurations.

Keywords Indian Monsoon · Global Climate Model ·
42 Low Pressure Systems · Air-sea coupling · Horizontal
43 resolution
44

1 Introduction

Air-sea coupling and horizontal resolution are generally
46 considered important for accurate simulations of cli-
47 mate and its components, for example the South Asian
48 Summer Monsoon (SASM). In this paper the hypo-
49 thesis is tested that they are important for synoptic-scale
50 monsoon depressions and lows, which are important
51 phenomena of the SASM. These systems contribute sub-
52 stantially to seasonal rainfall totals over the Indian sub-
53 continent, while also causing many of the extreme rain-
54 fall events during the summer monsoon season (Sikka
55 1977; Krishnamurthy and Ajayamohan 2010; Praveen
56 et al. 2015; Hunt et al. 2016); therefore their realistic
57 representation is essential for climate predictions and
58 projections on a range of time-scales.

The simulation of monsoon LPS in current climate
59 models is often poor (Ashok et al. 2000; Sabre et al.
60

Richard C. Levine · Gill M. Martin
Met Office Hadley Centre
Exeter, UK
E-mail: richard.levine@metoffice.gov.uk

Nicholas P. Klingaman · Simon C. Peatman
National Centre for Atmospheric Science-Climate
Department of Meteorology
University of Reading, Reading, UK

2000; Stowasser et al. 2009; Praveen et al. 2015; Levine and Martin 2018), with a deficient number of LPS and associated rainfall. In atmosphere-only models this may relate to the lack of air-sea coupling, which is important in other aspects of monsoon variability (as discussed below), or to coarse horizontal resolution. An increase in horizontal resolution may provide finer-scale detail that may help to improve the organization and propagation of LPS. However, including air-sea coupling and increasing resolution also substantially increase the complexity and expense of climate model simulations, therefore it is important to understand their individual effects.

Air-sea coupling is important in determining the formation, intensity and pathway of (Indian Ocean) tropical cyclones in climate models (eg. Subrahmanyam et al. 2005). It has also been shown to be important for the climate-model simulation of monsoon interannual variability (eg. Shukla and Huang 2016 and references therein) and intra-seasonal variability, including the onset vortex (Wu et al. 2012). Air-sea coupling and intra-seasonal sea surface temperature (SST) variability support the northward propagation of the boreal summer intra-seasonal oscillation (BSISO) that is associated with monsoon active-break cycles (Fu and Wang, 2004; DeMott et al. 2014), with coupling resulting in improvements to the relationship between SST and atmospheric convection, and contributes via the effect of high-frequency SST variability on surface fluxes to an estimated 20 % of the propagation of convection that is involved in the northward component of the BSISO (Gao et al. 2019). The prevalence and strength of monsoon depressions is highly correlated with active-break cycles (Krishnamurthy and Shukla, 2007), which suggests air-sea coupling may be important for the simulation of LPS, which often form, intensify and propagate over the warm summer Bay of Bengal (BoB) SSTs (Sikka 1977). Air-sea coupling may also reduce the intensity of monsoon LPS, due to local negative thermodynamic feedbacks on atmospheric convection that have been found to reduce extreme rainfall over the tropics in a similar coupled modelling setup as used in this study (Hirons et al. 2018). These feedbacks weaken local intense convection via reducing atmosphere-to-ocean net surface heat fluxes and increasing near-surface wind speeds, which cool the SST, reduce latent and sensible heat fluxes, and thereby weaken convection.

Coupled atmosphere-ocean configurations of the Met Office Unified Model (MetUM) generally show an increase in LPS over their atmosphere-only equivalents. However, the realistic effects of air-sea coupling alone are difficult to establish due to the development of substantial SST biases in coupled climate models, which

are especially wide-spread over the northern and equatorial Indian Ocean, both of which substantially affect the mean state atmospheric monsoon (Levine et al. 2013; Levine and Turner 2012; Bollasina and Ming 2013; Bollasina and Nigam 2009), thereby highlighting the importance of correctly representing air-sea coupled feedbacks. Coupled model SST biases have also been shown to negatively affect tropical sub-seasonal variability, including the Madden-Julian Oscillation (MJO) (Klingaman and Woolnough (2014), DeMott et al. 2015) and tropical cyclones (eg. Hsu et al. 2019), and therefore may also impact monsoon LPS.

In order to minimise the effect of coupled model SST biases, new simulations are analyzed using a configuration of the MetUM atmosphere model coupled to many columns of a mixed-layer ocean (MetUM-GOML2), whereby ocean temperature and salinity, and therefore also SSTs, are constrained to an observed mean seasonal cycle via corrections (Hirons et al. 2015). Furthermore, the one-dimensional ocean model allows air-sea coupling to be applied globally or in specific regions, allowing separation of the contributions from local and remote air-sea interactions to the representation of monsoon LPS. A further key advantage is that when the horizontal resolution of the ocean and atmosphere change, the oceanic mean state remains consistent, because the oceanic mean state is constrained to observations by prescribed temperature and salinity corrections. This allows separation of the effects on monsoon LPS from changes to resolution, and from changes in the oceanic mean state. This is not possible in a fully coupled atmosphere-ocean model, where a change in resolution will also change the oceanic and atmospheric mean state.

Compared to a fully coupled atmosphere-ocean model, the MetUM-GOML2 model lacks ocean dynamics, an important factor in SST variability. However, on synoptic to sub-seasonal time-scales that are of interest to monsoon LPS, the SST variability over the Indian Ocean is largely controlled by thermodynamic processes (e.g., Halkides et al 2015). The technique of applying temperature and salinity corrections in MetUM-GOML2 could also be applied to a fully coupled atmosphere-ocean model, but the presence of interactive ocean dynamics can complicate the results as the ocean dynamical response may lead the ocean model to drift away from the desired ocean mean state. In MetUM-GOML2, the lack of an ocean dynamical feedback to the corrections allows the effective use of imposed fixed corrections. This method is not a relaxation; it is a prescribed seasonal cycle of correction terms that are obtained from an initial, separate relaxation simulation (which is not analysed in this study; see Hirons et al. 2015 for details).

168 These MetUM-GOML2 simulations have previously
169 been used by Peatman and Klingaman (2018) to invest-
170 igate the influence of air-sea coupling and horizontal
171 resolution on the mean Indian summer monsoon and
172 its sub-seasonal variability. While coupling over the In-
173 dian Ocean degrades the atmospheric mean state due
174 to the presence of small remaining SST biases, there
175 are some improvements to the northward propagation
176 of the BSISO. Increasing the horizontal resolution from
177 200km to 90km improves the simulation of monsoon
178 rainfall and circulation, but there are no further im-
179 provements when the resolution is increased again to
180 40km. The improvements to the intra-seasonal variabil-
181 ity from increasing the resolution from 200km to 90km
182 are found to be of similar magnitude to the improve-
183 ments due to air-sea coupling over the Indian Ocean.

184 Previous work using an older version (Global At-
185 mosphere (GA) 3, described in Walters et al. 2011) of
186 the MetUM regional climate model (RCM) atmosphere-
187 only configuration suggested that the representation of
188 monsoon LPS can be substantially improved if biases in
189 the large-scale flow into the Indian monsoon area are
190 corrected (Levine and Martin 2018), while increasing
191 the horizontal resolution from 50km to 12km has lit-
192 tle effect (Karmacharya et al. 2016). Analysis of global
193 atmosphere-only model simulations at the same Me-
194 tUM version (GA3) has suggested little sensitivity of
195 monsoon LPS to increasing the horizontal resolution
196 from N96 (200km) up to N512 (40km) (Johnson et al.
197 2016). A newer version of the MetUM (GA6, described
198 in Walters et al. 2017), including the new dynamical
199 core ENDGAME, is used in this study, which may ex-
200 plain any difference in sensitivities.

201 While increased horizontal resolution may be ben-
202 efitial, as seen for example in analysis of monsoon de-
203 pression case studies in Numerical Weather Prediction
204 (NWP) simulations (Hunt and Turner 2017), the stud-
205 ies discussed above suggest that improving the overall
206 tropical circulation in the GCM at the standard hori-
207 zontal resolution would most improve our represen-
208 tation of monsoon LPS. In this case the improved repres-
209 entation of mean SST and the monsoon circulation as
210 a whole in MetUM-GOML2 found with increased reso-
211 lution and air-sea coupling (Peatman and Klingaman,
212 2018) may benefit monsoon LPS as well. It is interest-
213 ing to note that in most MetUM GCM experiments,
214 and also in the general development cycle of the Me-
215 tUM GCM, the strength of the mean state atmospheric
216 monsoon circulation (and rainfall) is always positively
217 correlated with the number of LPS (and their associ-
218 ated rainfall), which is also supported by CMIP5 anal-
219 ysis (Praveen et al. 2015). Levine and Martin (2018)
220 suggest that a stronger mean monsoon would increase

221 monsoon LPS, while there may be a positive feedback
222 with more and stronger monsoon LPS strengthening
223 the larger-scale flow into the region.

224 This study aims to establish whether increasing hori-
225 zontal resolution, using a range typical of current GCMs,
226 and the inclusion of a simple form of air-sea coupling,
227 over an atmosphere-only model, improves the forma-
228 tion, trajectories and associated rainfall of monsoon
229 LPS.

230 2 Simulations and data

231 The simulations use the GA6 configuration of the Me-
232 tUM atmosphere model (Walters et al. 2017).

233 Atmosphere-only experiments forced with observed
234 SST use the AMIP methodology (Gates et al. 1998)
235 and are forced with daily SST and sea-ice fractions from
236 Reynolds et al. (2007). Fully coupled atmosphere-ocean
237 MetUM present day control simulations use the GC2
238 configuration (Williams et al. 2015).

239 The mixed-layer ocean coupling experiments use the
240 MetUM-GOML2 configuration (Hirons et al. 2015), where
241 the vertical profiles of ocean temperature and salinity
242 are constrained using a prescribed seasonal cycle of cor-
243 rections. For all MetUM-GOML2 simulations analysed
244 here, the ocean is constrained to the 1980-2009 clim-
245 atology from Met Office ocean analyses (Smith and Mur-
246 phy, 2007). The coupling can be applied selectively in
247 space, and thereby allows coupling in individual ocean
248 basins only without substantial changes to the ocean
249 mean state. The resulting coupled simulations thereby
250 minimize the effects of changes in mean SST on the
251 atmosphere, although they still contain small SST bi-
252 ases (typically less than $\pm 0.5^{\circ}\text{C}$, although locally can
253 be over $\pm 1.0^{\circ}\text{C}$; see Peatman and Klingaman (2018)).
254 Due to limitations with regard to sea-ice cover, the cou-
255 pling is applied over the approximate latitude band
256 of 60°S - 60°N (see Hirons et al. 2015, Figure 2). The
257 lack of ocean dynamics means there is no representa-
258 tion of El Nino Southern Oscillation (ENSO) or Indian
259 Ocean Dipole (IOD) variability in the ocean (Hirons
260 et al. 2015). An indication of intraseasonal variabil-
261 ity of SST in MetUM-GOML2 for 90km simulations (the
262 higher horizontal resolution used in this study) is shown
263 by Peatman and Klingaman (2018) (their Fig. 7). This
264 shows that MetUM-GOML2 underestimates intrasea-
265 sonal variability in most of the tropical Indian Ocean,
266 with the strongest biases on the equator and in the
267 Arabian Sea. These are both regions where ocean dy-
268 namics (upwelling) are important for SST variability. In
269 the BoB, where most LPSs form and intensify, biases in
270 intraseasonal SST variability are smaller and consistent
271 with those in fully coupled GCMs.

Further, we note that the SST variability in the free-running MetUM-GOML2 simulation analysed here does not depend on the nudging timescale applied in the initial relaxation simulation (which is not analysed in this study). The free-running MetUM-GOML2 coupled simulations are corrected only by the mean seasonal cycle of temperature and salinity corrections from the relaxation simulations. Because these are fixed corrections, not a relaxation, the corrections do not damp SST variability. Indeed, Hiron et al. (2015) noted that shortening the relaxation timescale would increase the mean bias in the free-running simulation.

Simulations at N96 (longitude x latitude: $1.875^{\circ} \times 1.25^{\circ}$, approximately 200km at equator) and N216 ($0.83^{\circ} \times 0.55^{\circ}$, approximately 90km at equator) horizontal resolutions are compared. The simulations analysed are summarised in Table 1, and the notation for the simulations is discussed in the caption. Where SSTs from coupled model simulations have been used to force atmosphere-only simulations a 31-day smoothing has first been applied, following recommendations from DeMott et al. (2015). In simulations where coupling is applied regionally, climatological monthly-varying SST from Met Office ocean analyses (Smith and Murphy, 2007) are prescribed outside the coupled region. This means it is necessary to take account of interannual SST variability that is not present in the uncoupled regions, but is present in the globally coupled simulation and atmosphere-only simulation forced with either observed SST or SST from the globally coupled simulation. It is important to emphasize that the coupled regions in the MetUM-GOML2 simulations do have interannual variability in SST, however, this does not organise into coupled modes like ENSO or the IOD.

The 31-day smoothing to coupled model SSTs is recommended by DeMott et al. (2015) as it has been found that applying high-frequency (e.g., daily) SST forcing in an atmosphere-only global climate model (AGCM) leads to erroneous feedbacks between surface fluxes, SSTs and convection that amplify the rainfall response to SSTs and complicate the analysis of synoptic and sub-seasonal variability. In particular, AGCM convection parametrisations respond strongly and quickly to SST variability, such that in an AGCM, high-frequency warm SST anomalies are collocated with enhanced surface fluxes and high precipitation; high-frequency cold SST anomalies are collocated with reduced surface fluxes and low precipitation. The 31-day smoothing approach is further justified by the work of Hiron et al. (2018), who demonstrated that an AGCM with high-frequency SSTs overestimated precipitation extremes, relative to satellite-derived responses.

Tracking of monsoon LPS is carried out using TRACK software (Hodges 1994) with additional criteria specifically for Indian monsoon LPS following the methodology described in Levine and Martin (2018). The tracking is carried out by first filtering the vorticity data to a common T42 resolution in all cases, therefore there is no resolution dependence in the tracking method (Hodges 1994; Levine and Martin 2018).

ERA5 (ERA5; Copernicus Climate Change Service (C3S) (2017)) re-analysis data of 850hPa winds on a 6-hourly time-scale and at $0.25^{\circ} \times 0.25^{\circ}$ horizontal resolution are used for diagnosing monsoon LPS in observations and monthly mean ERA5 data for atmospheric winds, temperature and relative humidity are used for model comparison. Observational data for precipitation are taken from the APHRODITE data-set (Yatagai et al. 2009), as this has sufficiently high temporal (daily) and spatial (0.25°) resolution, although does not include coverage over the ocean, and currently only reaches up to 2007. Therefore, the observational data of the LPS tracks is analysed for the 1983-2007 period, which is still sufficient to compute a climatological average of monsoon LPS rainfall for comparison with the model data. GPCP monthly mean precipitation is used for evaluating the wider area mean conditions in the simulations (Adler et al 2003).

3 Results

3.1 Reanalysis and observations

We start by discussing the LPS detected in the ERA5 re-analysis, before moving to a comparison with the model simulations. Properties of these tracks combined with APHRODITE rainfall data are shown in Fig. 1. The track density in this figure is calculated as

$$\rho_{i,j} = \left[\sum_t \delta_{i,j,t} \right] / \left[\sum_{i,j} \sum_t \delta_{i,j,t} \right] \quad (1)$$

where $\delta = 1$ if a track is present at (i, j, t) or $\delta = 0$ otherwise, for all 6-hourly time-steps during LPS lifetimes. The coordinates i , j and t represent longitude, latitude and time respectively. Genesis density is calculated in a similar fashion:

$$\phi_{i,j} = \left[\sum_{\text{LPS}} \delta_{i,j,t_0} \right] / \left[\sum_{i,j} \sum_{\text{LPS}} \delta_{i,j,t_0} \right] \quad (2)$$

where t_0 is the first time-step for each LPS.

There are 212 LPS diagnosed in ERA5 in the 1983-2007 period during June to September, which is equivalent to almost 8.5 systems per monsoon season. The

Table 1 List of simulations. *ATM* represents an atmosphere-only simulation. *GL* represents the MetUM-GOML2 globally coupled simulation. Regionally coupled MetUM-GOML2 simulations are represented by *IO* (Indian Ocean), *PO* (Pacific Ocean), *AO* (Atlantic Ocean), *IO_PO* (Indian and Pacific Oceans), etc. *GC2* represents the fully coupled MetUM-GC2 configuration simulation. Sub-scripts show the horizontal resolution in km (either 200km or 90km). The value in brackets for atmosphere-only simulations indicates the SST used ([*obs*] for observational SST, [*GL*] for MetUM-GOML2 globally coupled SST, [*IO*] for MetUM-GOML2 Indian Ocean coupled SST, etc.)

Description	Atmosphere-Ocean Coupling	(MetUM) Resolution	Years
<i>ATM</i> ₂₀₀ [<i>obs</i>]	None - AMIP run (obs SST)	200km (N96)	1983-2010
<i>ATM</i> ₉₀ [<i>obs</i>]	None - AMIP run (obs SST)	90km (N216)	1983-2010
<i>GC2</i> ₂₀₀	Fully 3D coupled MetUM	200km (N96)	28 years (present day control run)
<i>GC2</i> ₉₀	Fully 3D coupled MetUM	90km (N216)	28 years (present day control run)
<i>GL</i> ₂₀₀	GOML2 Global (constrained to obs)	200km (N96)	28 years
<i>AO_PO</i> ₂₀₀	GOML2 Global, EXCEPT Indian Ocean	200km (N96)	28 years
<i>IO</i> ₂₀₀	GOML2 Indian Ocean only	200km (N96)	28 years
<i>PO</i> ₂₀₀	GOML2 Pacific Ocean only	200km (N96)	28 years
<i>IO_PO</i> ₂₀₀	GOML2 Indian and Pacific Oceans	200km (N96)	28 years
<i>ATM</i> ₂₀₀ [<i>IO</i>]	None – SSTs from <i>IO</i> ₂₀₀ (31-day smoothed)	200km (N96)	28 years
<i>ATM</i> ₂₀₀ [<i>GL</i>]	None - SSTs from <i>GL</i> ₂₀₀ (31-day smoothed)	200km (N96)	28 years
<i>GL</i> ₉₀	GOML2 Global (constrained to obs)	90km (N216)	28 years
<i>AO_PO</i> ₉₀	GOML2 Global EXCEPT Indian Ocean	90km (N216)	28 years
<i>IO</i> ₉₀	GOML2 Indian Ocean only	90km (N216)	28 years
<i>PO</i> ₉₀	GOML2 Pacific Ocean only	90km (N216)	28 years
<i>IO_PO</i> ₉₀	GOML2 Indian and Pacific Oceans	90km (N216)	28 years
<i>ATM</i> ₉₀ [<i>IO</i>]	None - SSTs from <i>IO</i> ₉₀ (31-day smoothed)	90km (N216)	28 years
<i>ATM</i> ₉₀ [<i>GL</i>]	None - SSTs from <i>GL</i> ₉₀ (31-day smoothed)	90km (N216)	28 years
<i>ERA5/APHRO</i>	atm U, V, T, RH from re-analysis / obs land-only precip	0.25° / 0.25°	1983-2007

systems mainly originate in the northern Bay of Bengal, with further systems developing within the monsoon trough over north eastern India. During the early monsoon a small number of cyclonic systems develop over the eastern Arabian Sea. The combined effects of the LPS contribute a substantial amount of rainfall to the north-eastern and northern areas of India.

3.2 Standard MetUM simulations and MetUM-GOML2 SST biases

In this section results are presented from standard AMIP-style atmosphere only simulations forced with observed SST (*ATM*[*obs*]) and fully coupled atmosphere-ocean simulations (*GC2*). The *GC2* simulations have substantial SST biases, both local and remote to the Indian Ocean sector (eg. Fig. 2a in Wainwright et al. 2019). Effects of local Indian Ocean SST biases on the Indian monsoon have been shown for a previous version of the MetUM in Levine and Turner (2012), with northern Indian Ocean and equatorial Indian Ocean cold SST biases having counteracting effects. However, the cold SST bias over the Arabian Sea dominated in that particular version of the model, resulting in weakened monsoon winds and rainfall. This pattern of cold SST biases, although smaller in magnitude, is still persistent in the *GC2* configuration used in this study, but it appears that there is less influence from the cold bias over the Arabian Sea.

The SST biases in the MetUM-GOML2 simulations discussed in this study are shown in Fig. 2. This shows that there is still a cold SST bias present over the

equatorial Indian Ocean at both horizontal resolutions, which may influence the Indian monsoon and LPS. A direct impact of this could be to strengthen the monsoon circulation, as expected from experiments using a previous configuration of the MetUM (Levine and Turner, 2012). However, differences in the magnitude or area of the SST bias may result in other impacts, while other models may behave differently (Ballasina and Nigam 2009; Prodhomme et al. 2014). There is also the potential for remote SST biases over the Atlantic or Pacific Oceans to influence the monsoon indirectly through atmospheric teleconnections.

The cold SST biases in the Indian Ocean are primarily the result of errors in atmospheric wind-stress forcing of the ocean, which cannot be eliminated using the temperature and salinity corrections. Excessive wind-driven oceanic vertical mixing cools SST, but also means that the temperature corrections applied are too readily mixed. The temperature corrections attempt to restratify the ocean and shoal the mixed layer – by warming near the surface and cooling at depth – but these corrections are ineffective as they are mixed across the (deeper) mixed layer by the atmospheric wind forcing. The strength of the cold SST biases does not depend strongly on the nudging timescale used in the initial MetUM-GOML2 relaxation simulation. Shortening the nudging timescale would strengthen the temperature corrections, but retain their vertical profile – warming near the surface and cooling at depth – resulting in nearly zero net change to oceanic heat content and hence similar biases in SST and mixed-layer depth. For further details, see Hiron et al. (2015).

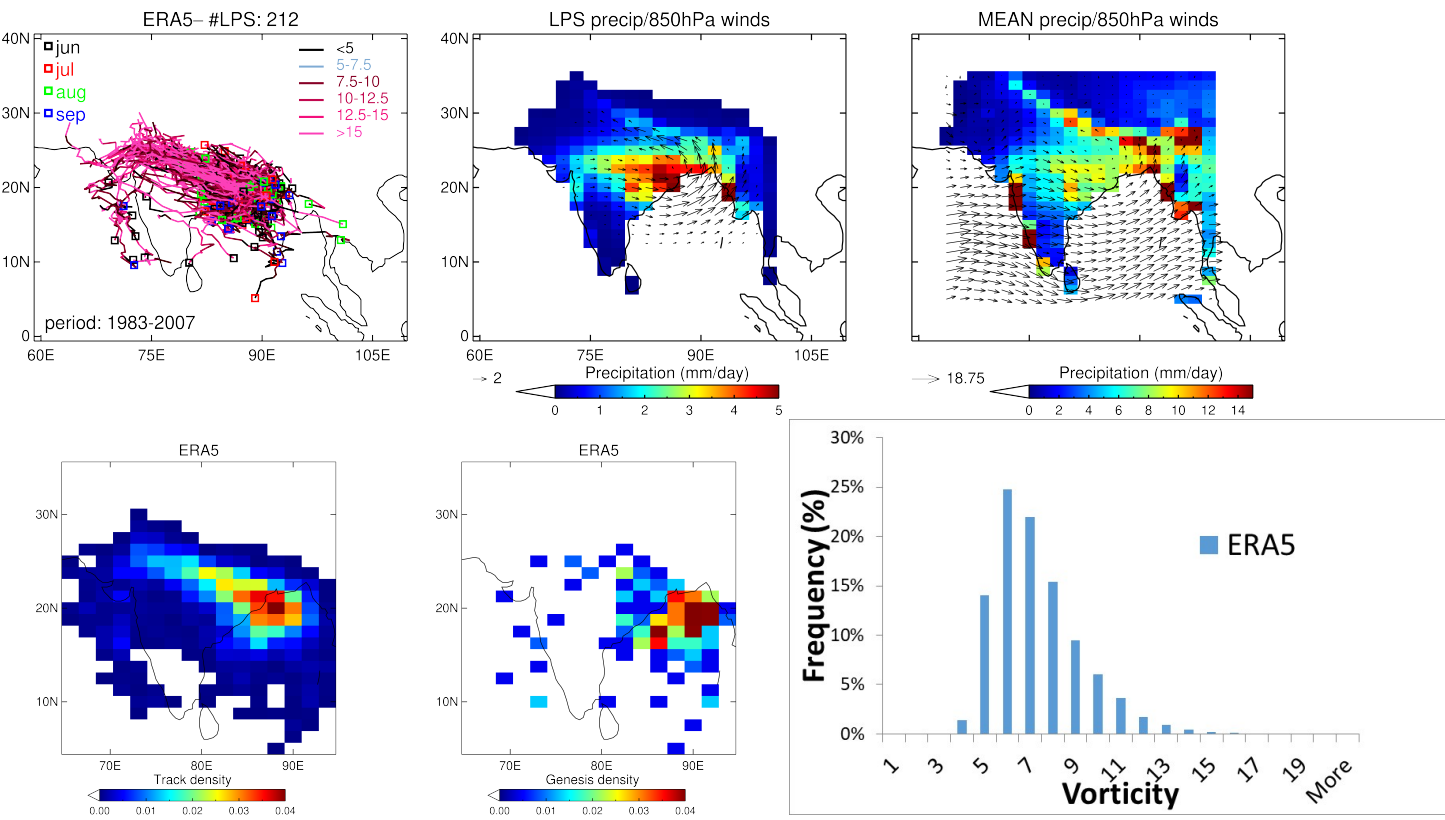


Fig. 1 Monsoon LPS diagnosed in ERA5 re-analysis for 1983-2007 with APHRODITE land precipitation statistics. On the top row: the *first panel on left hand-side* shows LPS trajectories with the total number of LPS in title. The coloured squares indicate the starting point and month of each track. The colour of the trajectories indicates the strength in terms of relative vorticity ($10^{-5} s^{-1}$ at native resolution). The *second panel from left* shows LPS contribution to JJAS seasonal mean precipitation (mm/day) and 850 hPa winds (m/s, black vectors). The *third panel from left* shows Jun-Sept seasonal mean precipitation (mm/day) and 850 hPa winds (m/s, black vectors). All data is plotted on a 200km (N96; $1.875^\circ \times 1.25^\circ$) grid. Bottom row shows TRACK DENSITY, GENESIS DENSITY and a HISTOGRAM of LPS intensity. The intensity is shown in terms of relative vorticity (in units of $10^{-5} s^{-1}$) filtered to T42 resolution (as used in tracking) at the centre of the system at the 850hPa level, and includes all 6-hourly time-steps during LPS lifetime. These ERA5 figures have been generated using Copernicus Climate Change Service Information 2020.

The results of LPS analysis for $ATM_{90}[obs]$, GC_{90} , GL_{90} and $ATM_{90}[GL]$ are shown in Fig. 3. An equivalent comparison for the 200km (N96) simulations has qualitatively similar results and is not shown. The MetUM simulations have substantially less LPS activity than ERA5, while activity is far more spatially limited to the Bay of Bengal, with only a few systems travelling westwards across India in the monsoon trough. This lack of LPS in global simulations, and the inability to propagate over Indian land, is a typical feature of MetUM climate configurations (Levine and Martin, 2018). The $ATM_{90}[obs]$ has only 76 LPS, or 2.7 LPS per season, which is approximately 32% of the number in ERA5. This coincides with the consistently weak monsoon in the MetUM (e.g. Johnson et al. 2016). The fully coupled GC_{290} simulation has a few more systems and associated LPS rainfall, which coincides with stronger westerly low-level winds across the Arabian

Sea, India and the Bay of Bengal. There is also more rainfall across this band, although not much over Indian land. Differences between GC_{90} and $ATM_{90}[obs]$ could be due to many factors, including direct effects of coupling on LPS, local or remote effects of coupling on the monsoon circulation, direct effects of local SST biases on LPS, or local or remote effects of SST biases on the monsoon circulation.

The MetUM-GOML2 mixed-layer ocean coupled simulation GL_{90} shows quite similar changes to GC_{290} , though there are now substantially more systems (4.4 on average per season, or approximately half of the number in ERA5). This coincides with more LPS rainfall, which now also starts to show some impact on mean rainfall over NE India. There could be numerous reasons for the differences with GC_{290} , for example a local impact could be the strengthening of the monsoon circulation due to a change in the balance of northern

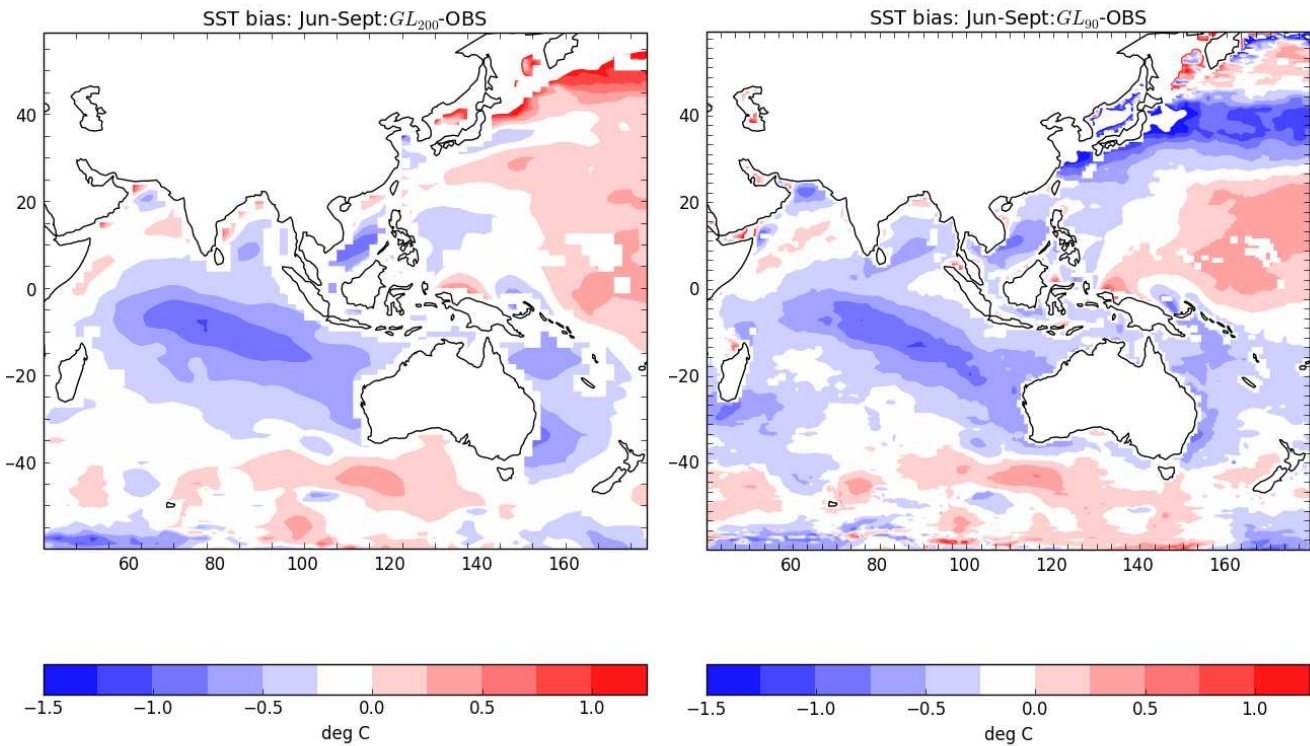


Fig. 2 Climatological JJAS SST biases for GL_{200} and GL_{90} compared to Smith and Murphy (2007) observations.

and equatorial Indian Ocean SST biases, thereby providing more favourable conditions for LPS formation. The comparison with $ATM_{90}[GL]$ allows some more definite conclusions on the effects of SST biases. The $ATM_{90}[GL]$ simulation is very close to GL_{90} in terms of differences with the $ATM_{90}[obs]$ standard AMIP-type simulation. This suggests that coupling is not a major influence in the changes seen in the latter three rows of 3 with respect to $ATM_{90}[obs]$, which therefore are quite likely the result of SST biases. It should be noted that the AMIP-type runs also contain variability due to ENSO and IOD events in the SST forcing, while the atmosphere-only runs forced with the coupled SST do not contain such variability due to the smoothing applied. This is likely to affect the interannual variability in LPS and may also affect the mean number of LPS due to non-linear effects.

It is also worth noting that Peatman and Klingaman (2018) has investigated the role of intra-seasonal variability (ISV), interannual variability (IAV) and SST biases in differences in the mean state atmosphere presented due to coupling in different basins, and it is concluded that these are mainly attributable to SST biases. The $GL - AO_PO$ differences (Peatman and Klingaman (2018), Figs. 3a,c) then give an approximation of the effects of Indian Ocean SST biases, which are to cause a

relative reduction of precipitation over the equatorial Indian Ocean and increase to the north of this, while there are no significant changes over Indian land. This is accompanied by strengthening of the low-level monsoon jet starting from the Bay of Bengal and extending through the South China Sea into the W Pacific. While the latter is consistent with the effects seen in this study (Fig. 3, note different scales) in $ATM[GL] - ATM[obs]$, the biases in the mean state precipitation in this case are more widespread and larger than the aforementioned $GL - AO_PO$ changes in Peatman and Klingaman (2018), which must then be explained by effects of missing IAV and/or ISV in the $ATM[GL]$ experiments and possibly the role of any of these processes feeding back on each other.

The precise attribution of changes to the monsoon circulation and LPS to localised SST biases and their mechanisms is beyond the scope of this study. However, while the atmospheric monsoon base state may be slightly different from the standard fully coupled and AMIP-style MetUM simulations, the isolated comparison of MetUM-GOML2 mixed-layer ocean coupled simulations and their equivalent atmosphere-only simulations (forced with GOML2 SST) does provide for a somewhat idealised decomposition into effects from coupling and from resolution.

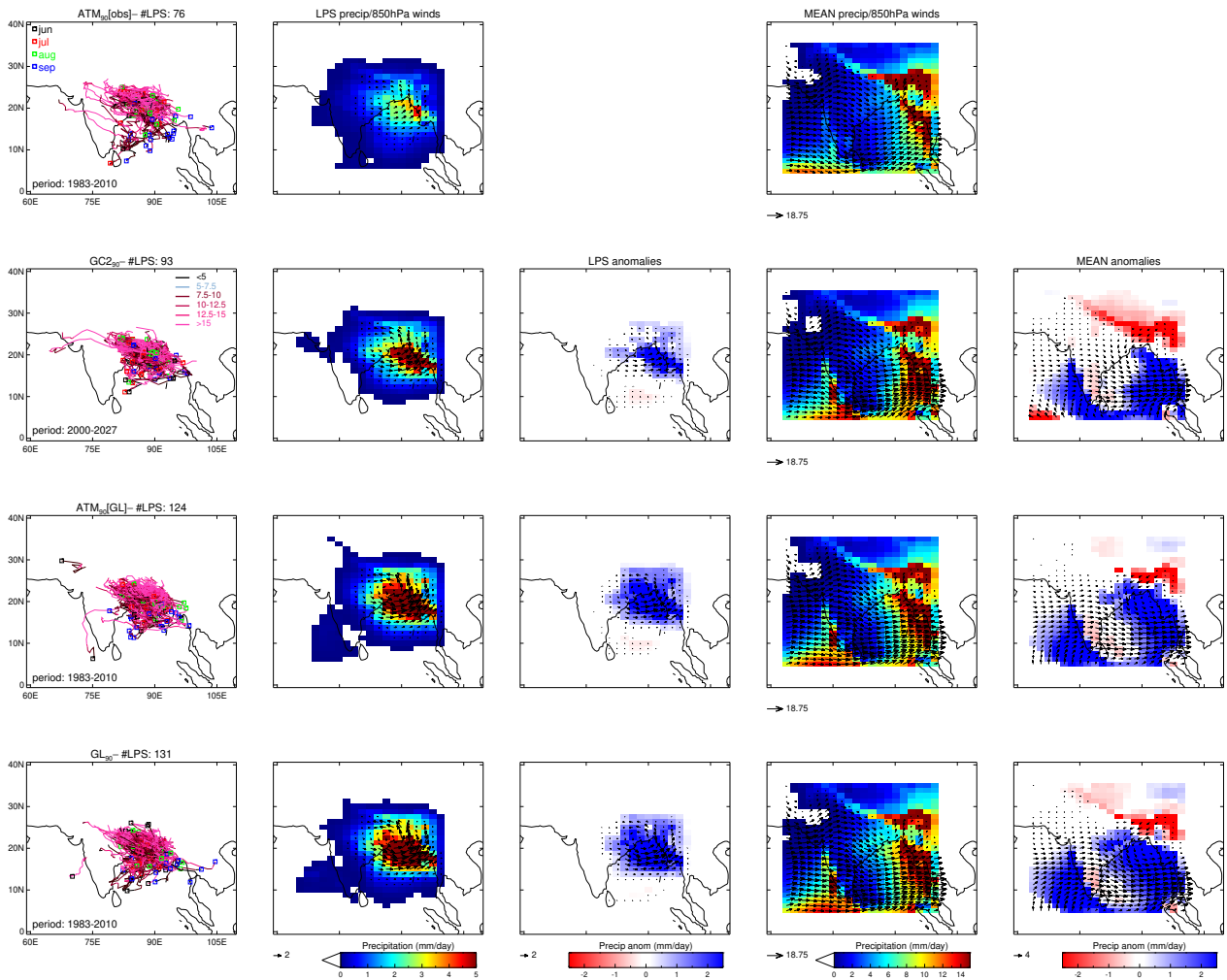


Fig. 3 Monsoon LPS diagnosed in 90km (N216) experiments for 1983–2010 period. Top row shows the *ATM₉₀[obs]* experiment, with subsequent rows showing results for *GC₂₉₀*, *GL₉₀* and *ATM₉₀[GL]*. Differences are all in comparison to *ATM₉₀[obs]*. The *first panel on left hand-side* shows LPS trajectories with the total number of LPS in title. The coloured squares indicate the starting point and month of each track. The colour of the trajectories indicates the strength in terms of relative vorticity (10^{-5} s^{-1} at native resolution). The *second panel from left* shows LPS contribution to JJAS seasonal mean precipitation (mm/day) and 850 hPa winds (m/s, black vectors). The *third panel from left* shows difference in LPS precipitation and 850hPa wind contributions with respect to top row experiment. The *fourth panel from left* shows Jun-Sept seasonal mean precipitation (mm/day) and 850 hPa winds (m/s, black vectors). The *fifth panel from left* shows difference in Jun-Sept seasonal mean and 850hPa wind contributions with respect to top row experiment. Data are plotted on a common 200km (N96; $1.875^\circ \times 1.25^\circ$) grid. Only significant differences and vectors at 90% level using a student t-test are shown. Values exceeding the colour scale maxima are capped at the relevant maximum colour value.

518 3.3 Role of air-sea coupling

519 In order to isolate the effects of the air-sea coupling,
 520 each coupled simulation is compared to the equivalent
 521 atmosphere-only simulation forced with (31-day smoothed)
 522 SSTs from the coupled simulation. In this way, for ex-
 523 ample, the *GL₂₀₀* simulation should be compared to
 524 *ATM₂₀₀[GL]*. However, we also compare against the
 525 atmosphere-only simulation forced with observed SSTs

526 in order to interpret the results from the regionally-
 527 coupled simulations.

528 3.3.1 Global coupling

529 The number of monsoon LPS in *GL₂₀₀* (81, equivalent
 530 to 2.9 LPS per JJAS season on average) and *ATM₂₀₀[GL]*
 531 (75, equivalent to 2.7 LPS per season on average) is
 532 similar, though there is an eastward shift visible in the
 533 location of the LPS trajectories and the resulting rain-

fall in GL_{200} (Fig. 4). In the coupled simulation the LPS appear to produce marginally less rainfall, while the trajectories and rainfall are somewhat more constrained over the Bay of Bengal and do not move as far westwards across northern India as in observations. This reduced rainfall over the monsoon trough helps explain the differences between these simulations in the mean seasonal JJAS rainfall, the main feature of which is weaker rainfall over much of India and the BoB in GL_{200} . The comparison of GL_{200} with $ATM_{200}[obs]$ in Fig. 4 further highlights that the combined effect of differences in interannual SST variability and SST biases in GL_{200} results in a strengthening of the seasonal mean monsoon and increased LPS activity in GL_{200} . This is an important consideration when interpreting the locally coupled simulations in later sections.

The percentage of seasonal rainfall change due to changes in LPS is shown in Fig. 5. This is calculated as

$$\Delta = 100\% \times \left[\frac{Pr_{LPS}(GL) - Pr_{LPS}(ATM[GL])}{Pr(GL) - Pr(ATM[GL])} \right], \quad (3)$$

where Pr is mean JJAS precipitation and Pr_{LPS} is LPS rainfall over the same period.

This highlights that the changes over India and the BoB are to a large degree attributable to LPS. The damping effect of air-sea coupling on LPS rainfall over the BoB is consistent with the localised effect of air-sea coupling on tropical rainfall seen in previous studies (eg. Hiron et al. 2018).

Both 200km (N96) MetUM simulations have substantially fewer LPS and less LPS rainfall than diagnosed in ERA5 and APHRODITE (cf. Fig. 1). The trajectories in the re-analysis also reach substantially further westwards across northern India within the monsoon trough. This lack of LPS in global simulations, and the inability to propagate over Indian land, is a typical feature of MetUM climate configurations (Levine and Martin, 2018).

These common biases in LPS representation with respect to observations/reanalysis are likely the result of the overall weak monsoon circulation in this configuration as also seen in AMIP-style simulations in previous configurations of the MetUM (eg. Johnson et al. 2016). The relatively weak Somali Jet, the lack of rainfall over India, the excessive rainfall over the equatorial Indian Ocean and Himalayan foothills are all part of this, and make for unfavourable conditions for LPS formation and westward propagation over the relatively dry Indian land. It has been shown in Levine and Martin (2018) using regional climate model simulations that substantial improvements are seen when the inflow conditions into the Indian sector are corrected, including the probable effect of pre-cursor disturbances from the W Pacific.

3.3.2 Coupling in individual basins

In this section the effect of coupling in individual basins is examined in the 200km (N96) simulations (Figure 6). Among these simulations, the global coupling experiment produces the most LPS, which appear to play a role in differences in seasonal-mean precipitation over Indian land. On the other hand, the experiments without coupling over the Indian Ocean produce the fewest LPS and least LPS rainfall, suggesting local coupling is important for Indian monsoon LPS formation.

The effects of coupling will be examined two ways, using two different reference states. The first uses GL_{200} as the reference simulation. In this way we examine the contribution to the overall effect of global coupling from the following four areas:

1. **Coupling INSIDE Indian Ocean only:** $GL_{200} - AO_PO_{200}$ (Fig. 6, second row),
2. **Coupling OUTSIDE Indian Ocean:** $GL_{200} - IO_{200}$ (Fig. 6, third row),
3. **Coupling OUTSIDE Pacific Ocean:** $GL_{200} - PO_{200}$ (Fig. 6, fourth row),
4. **Coupling OUTSIDE Indian and Pacific Oceans:** $GL_{200} - IO_PO_{200}$ (Fig. 6, fifth row).

The first of these ($GL_{200} - AO_PO_{200}$) indicates the effect of adding Indian Ocean coupling in comparison to a base state where (i) there is already air-sea coupling in the Atlantic and Pacific Oceans; (ii) there are MetUM-GOML2 mean SST biases in all three basins (Indian, Pacific and Atlantic Oceans); and (iii) there are no coupled modes of variability like ENSO or the IOD.

In general, the contribution from coupling over the Indian Ocean ($GL_{200} - AO_PO_{200}$) to the effects of global coupling on Indian monsoon LPS rainfall is similar, and of the same sign, to that from coupling outside the Indian Ocean ($GL_{200} - IO_{200}$). This suggests that both coupling within and outside the Indian Ocean have a positive effect of similar magnitude, which is particularly evident in monsoon LPS rainfall. In terms of JJAS mean rainfall, in addition to the effects over India and the BoB from the monsoon LPS, there is a more widespread positive effect from coupling within the Indian Ocean on rainfall over the Arabian Sea, BoB and equatorial Indian Ocean.

Of the other areas shown, there is a neutral effect from coupling outside the Indian and Pacific Oceans ($GL_{200} - IO_PO_{200}$). This suggests that the positive effects from coupling outside the Indian Ocean ($GL_{200} - IO_{200}$), as discussed earlier, are primarily due to effects of coupling over the Pacific Ocean. Furthermore, the effects of coupling outside the Pacific Ocean (GL_{200}

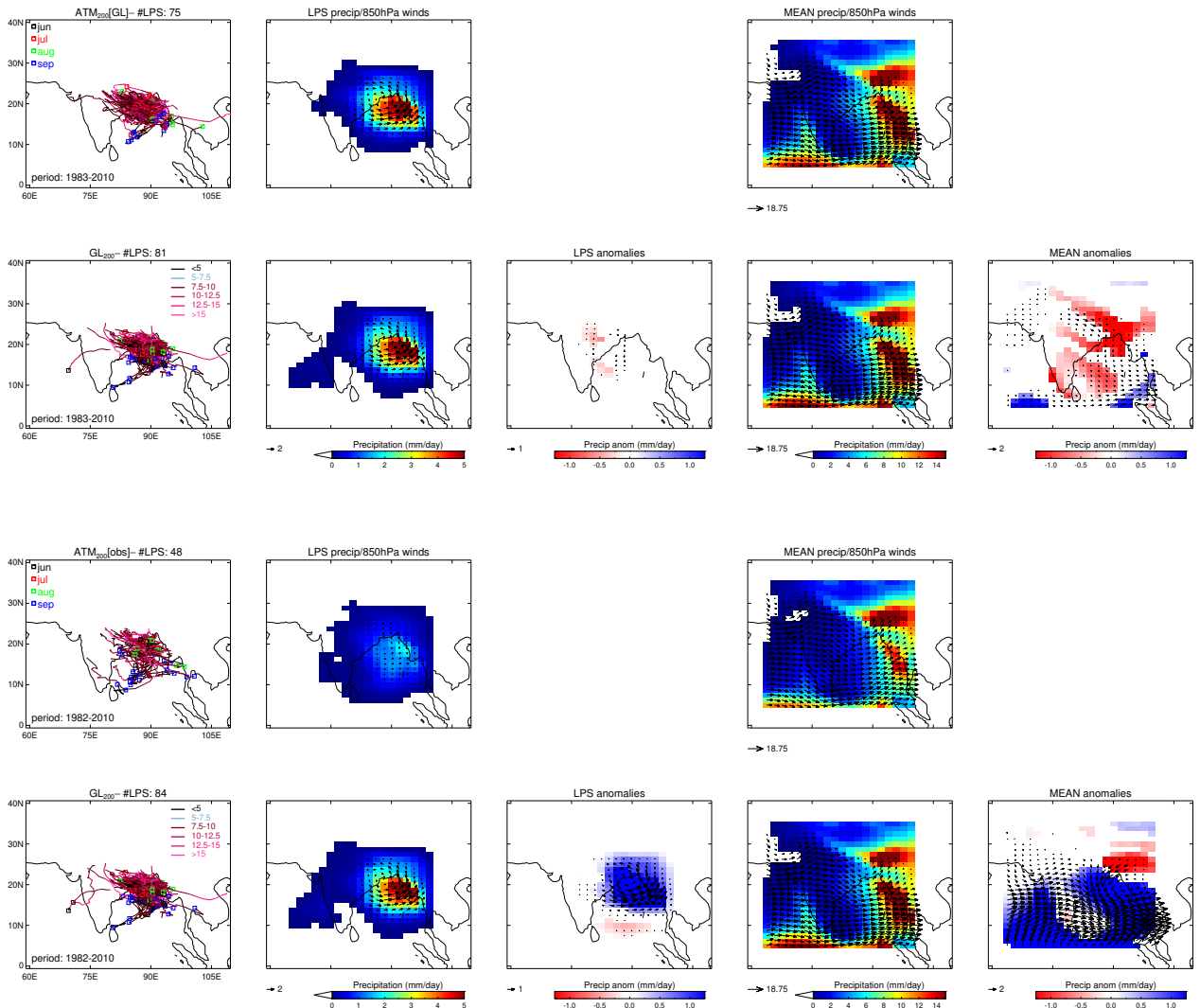


Fig. 4 Monsoon LPS diagnosed in 200km (N96) experiments for 1983-2010 period. Top row shows the $ATM_{200}[GL]$ experiment, second row shows the GL_{200} experiment, with differences displayed as $[GL_{200} - ATM_{200}[GL]]$. The same comparison is shown for GL_{200} with $ATM_{200}[obs]$ in the third and fourth rows. The **first panel on left hand-side** shows LPS trajectories with the total number of LPS in title. The coloured squares indicate the starting point and month of each track. The colour of the trajectories indicates the strength in terms of relative vorticity ($10^{-5} s^{-1}$ at native resolution). The **second panel from left** shows LPS contribution to JJAS seasonal mean precipitation (mm/day) and 850 hPa winds (m/s, black vectors). The **third panel from left** shows difference in LPS precipitation and 850hPa wind contributions with respect to top row experiment. The **fourth panel from left** shows Jun-Sept seasonal mean precipitation (mm/day) and 850 hPa winds (m/s, black vectors). The **fifth panel from left** shows difference in Jun-Sept seasonal mean and 850hPa wind contributions with respect to top row experiment. All data in panels two, three, four and five are plotted on a common 200km (N96; $1.875^\circ \times 1.25^\circ$) grid. Only significant differences and vectors at 90% level using a student t-test are shown. Values exceeding the colour scale maxima are capped at the relevant maximum colour value.

637 - PO_{200}) are very similar to the effects of coupling out-
 638 side the Indian Ocean (GL_{200} - IO_{200}).

639 However, it is important to note that these (ap-
 640 parent positive) effects are of the opposite sign to the
 641 GL_{200} - $ATM_{200}[GL]$ comparison, which suggested a
 642 neutral-negative effect of global coupling when refer-
 643 enced to the equivalent atmosphere-only simulation. This

644 discrepancy can occur due to various reasons. Firstly,
 645 the uncoupled regions in IO_{200} , PO_{200} , etc. are pre-
 646 scribed with climatological monthly-varying observed
 647 SST, which does not contain interannual SST variabil-
 648 ity that is present in the globally coupled simulation
 649 and the atmosphere-only simulation forced with SST
 650 from the globally coupled simulation. Secondly, the re-

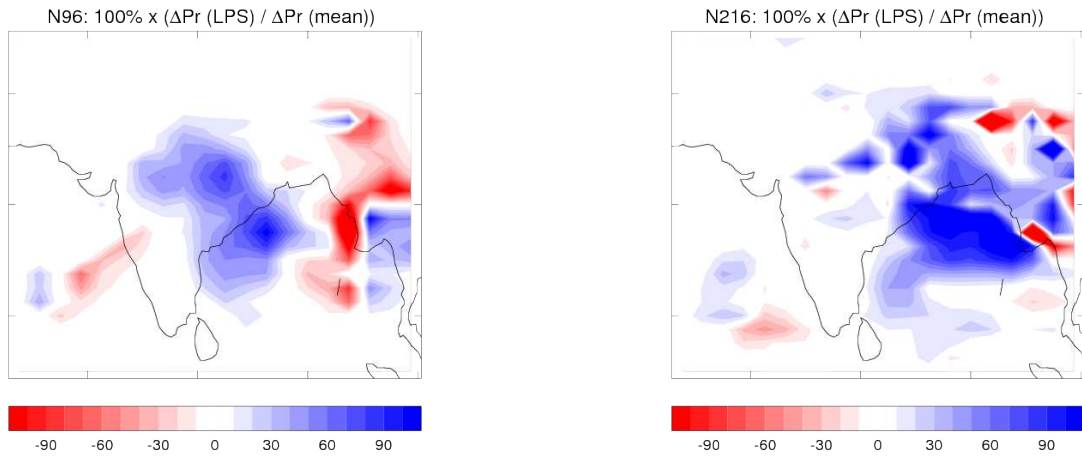


Fig. 5 Percentage of seasonal change in rainfall due to LPS in N96 (200km, on left) and N216 (90km, on right) global coupling experiments. Calculated as in eq. 3. Grid-boxes where mean precipitation change $|Pr(GL) - Pr(ATM[GL])| < 0.1$ mm/day have been masked out (set to zero). Note that values can exceed $\pm 100\%$ due to compounding/compensating changes in mean rainfall from sources other than LPS.

maining SST biases in the globally coupled simulation are not present in the uncoupled regions of the regionally coupled simulations. The $GL_{200} - ATM_{200}[obs]$ comparison in Fig. 4, which shows a strengthening of the monsoon and LPS in GL_{200} due to differences in interannual SST variability and SST bias, suggests that the positive signals found in the previous comparison of the locally coupled simulations may be (at least partly) for the same reason. Thirdly, there may be interaction between the effects of coupling in different basins. However, it should be emphasized that the first two factors do not affect the $GL_{200} - ATM_{200}[GL]$ comparison.

The second comparison uses $ATM_{200}[obs]$ as the reference simulation in order to examine the effect of coupling in each of the different regions versus no coupling at all. In this case the mean SST in the uncoupled regions (climatological monthly-varying observed SST from Met Office ocean analyses) remains relatively consistent in all the simulations with the observed SST from Reynolds et al. (2007) in the atmosphere-only AMIP-type run ($ATM_{200}[obs]$). Global coupling ($GL_{200} - ATM_{200}[obs]$) has already been shown in this manner in Fig. 4.

5. **Coupling INSIDE Atlantic and Pacific Oceans:** $AO_PO_{200} - ATM_{200}[obs]$ (Fig. 7, second row),
6. **Coupling INSIDE Indian Ocean only: $IO_{200} - ATM_{200}[obs]$** (Fig. 7, third row),
7. **Coupling INSIDE Pacific Ocean only: $PO_{200} - ATM_{200}[obs]$** (Fig. 7, fourth row),
8. **Coupling INSIDE Indian and Pacific Oceans: $IO_PO_{200} - ATM_{200}[obs]$** (Fig. 7, fifth row).

For example, the $IO_{200} - ATM_{200}[obs]$ comparison indicates the effect of adding Indian Ocean coupling

compared to a base state where (i) the Atlantic and Pacific Oceans are not coupled; (ii) the mean SST in the Atlantic and Pacific Oceans is similar to observed; and (iii) there are coupled modes of variability like ENSO present.

The results suggest that the combined Indian and Pacific Ocean coupling $IO_PO_{200} - ATM_{200}[obs]$ has the largest effect, similar but slightly weaker than the equivalent global coupling response $GL_{200} - ATM_{200}[obs]$ (Fig. 4), while the biggest single influence comes from Indian Ocean coupling. Differences between the two comparisons of coupling inside the Indian Ocean ($GL_{200} - AO_PO_{200}$ and $IO_{200} - ATM_{200}[obs]$) are relatively small, and may reflect the effect of differences in interannual SST variability between the reference simulations.

In summary, while there are the caveats with respect to differences in SST biases and variability, both comparisons point to the largest sensitivity coming from air-sea coupling in the Indian Ocean and Pacific Ocean basins.

3.4 Role of horizontal resolution

3.4.1 Impact of increase in horizontal resolution

The ATM_{90} and GL_{90} higher resolution simulations are compared to the observations in Fig. 8. The main feature is that the increase in resolution from 200km (N96) to 90km (N216) results in substantially more LPS activity and increased LPS rainfall (cf. Fig. 4). The number of monsoon LPS in GL_{90} is 131 (equivalent to 4.7 LPS per JJAS season on average), while $ATM_{90}[GL]$

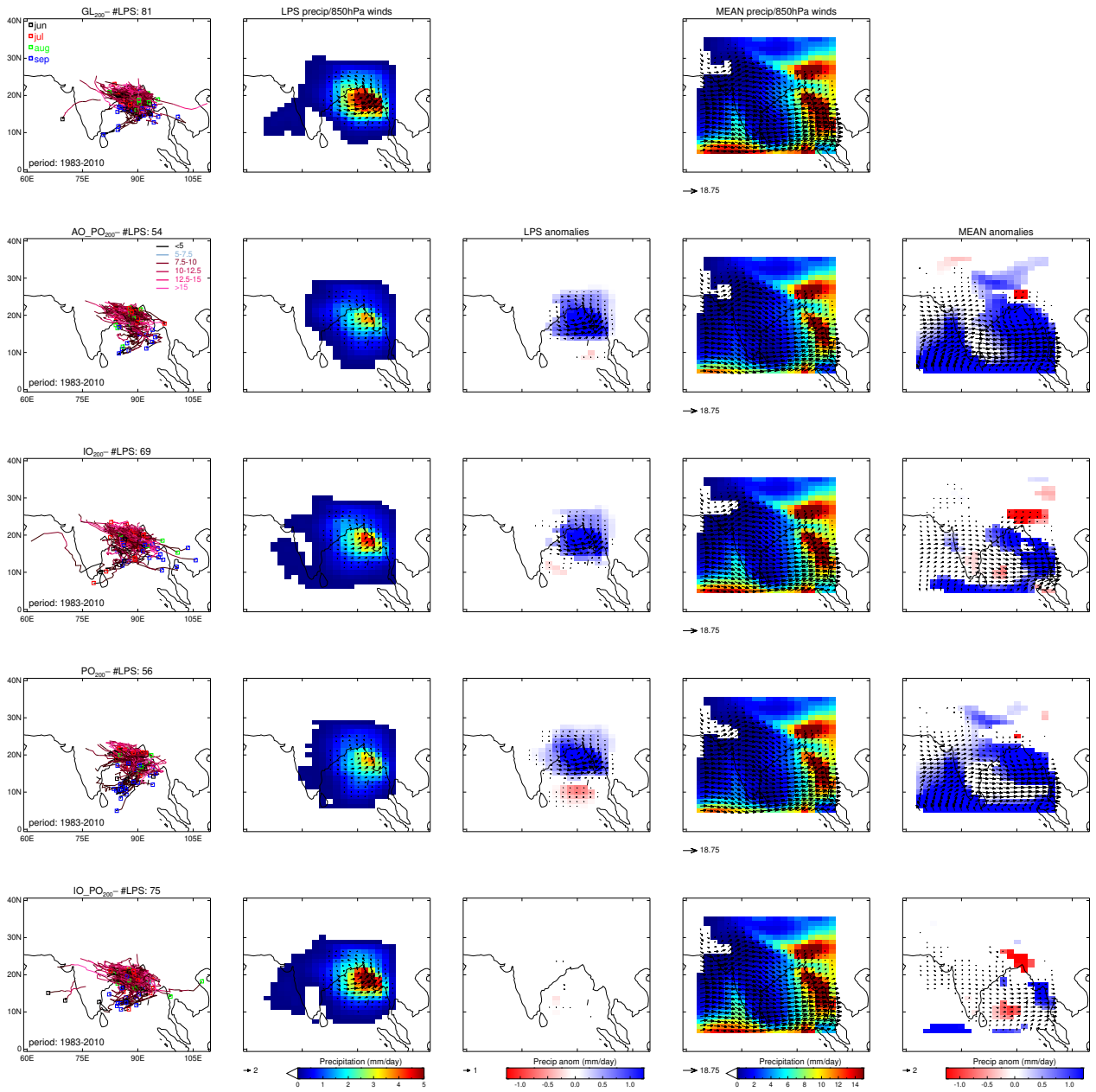


Fig. 6 Coupling sensitivity of 200km (N96) simulations for 1983-2010 period. Top row shows the Global Coupling (obs) experiment, while subsequent rows show the results for regional coupling and differences displayed as $[GL_{200} - AO.PO_{200}]$ (coupling INSIDE Indian Ocean), $[GL_{200} - IO_{200}]$ (coupling OUTSIDE Indian Ocean), $[GL_{200} - PO_{200}]$ (coupling OUTSIDE Pacific Ocean), $[GL_{200} - IO.PO_{200}]$ (coupling OUTSIDE Indian and Pacific Oceans). The layout of the plots is as described in Fig. 4.

714 has a similar number (124, equivalent to 4.4 LPS per
 715 season on average). These are closer to the observed
 716 number (6.8 per JJAS season) than the lower resolution
 717 200km (N96) simulations. As stated previously, the
 718 results from the LPS tracking are independent of resolution,
 719 therefore the improvements at higher resolution
 720 are due to the model capturing the LPS more accu-

721 rately. In both the atmosphere-only and coupled 90km
 722 (N216) simulations the systems form over a larger area
 723 of the BoB than is the case for the 200km (N96) sim-
 724 ulations, which is somewhat more in line with obser-
 725 vations. The LPS are also somewhat more realistic as
 726 they travel further north-westwards across the BoB and
 northern India at higher resolution.

721
 722
 723
 724
 725
 726

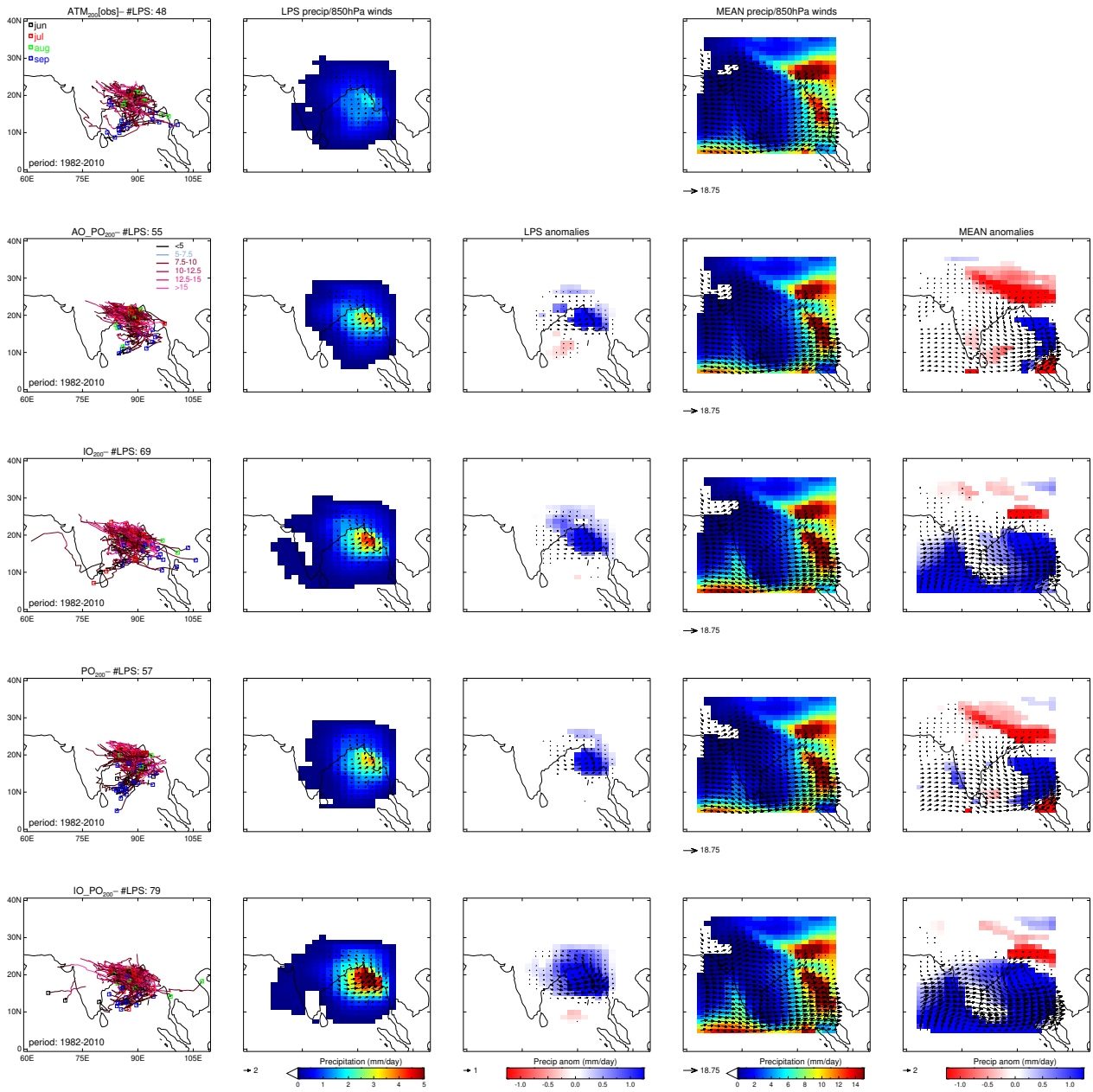


Fig. 7 Coupling sensitivity of 200km (N96) simulations for 1983-2010 period. Top row shows the Atmosphere-only experiment, while subsequent rows show the results for regional coupling and differences displayed in the following form $[IO200] - ATM200[obs]$. The layout of the plots is as described in Fig. 4.

728 There are several factors which likely combine to
 729 result in the improvements with increased horizontal
 730 resolution. Firstly, better resolving the structure of the
 731 LPS. Using the same MetUM configuration (GA6) using
 732 initialised NWP simulations of monsoon depressions,
 733 Hunt and Turner (2017) found the greatest im-
 734 provements with changes in horizontal resolution when
 735 moving from N96 (denoted in this paper as 200km)
 736 to N216 (denoted in this paper as 90km), with little

737 improvement beyond that. This indicates that there
 738 should be an improvement in resolving the structure
 739 of the LPS in our higher resolution simulations.

740 The second factor is improvement to the wider re-
 741 gion circulation. Levine and Martin (2018) and Karm-
 742 charya et al (2015, 2016), using an older configura-
 743 tion of the MetUM (GA3, without the ENDGAME dy-
 744 namic core improvements in GA6), found that hori-
 745 zontal resolution (in this case from 50km to 12km) plays

746 a smaller role than improving the wider region circulation,
 747 in particular the Somali Jet and pre-cursor disturbances
 748 from the W Pacific, in realistic representation of
 749 monsoon LPS. This was established using a series of
 750 regional climate models with different domains and forced
 751 with realistic boundary conditions from reanalysis. Im-
 752 provements to the larger-scale monsoon circulation, in
 753 particular to the Somali Jet, with increased hori-
 754 zontal resolution are found, for example, due to improved
 755 representation of East African orography (Johnson et
 756 al 2016), again using older GA3 configuration global
 757 climate simulations. In addition, as some pre-cursor
 758 disturbances from the east originate from typhoons or
 759 tropical storms in the South China Sea or beyond (Saha
 760 et al 1981), it is likely that these are represented more
 761 accurately at higher resolution (Roberts et al. 2020),
 762 which will again improve conditions for Indian mon-
 763soon LPS to form.

764 The effect of coupling at higher resolution (GL_{90} -
 765 $ATM_{90}[GL]$) seems mostly to amplify these changes,
 766 with more LPS and associated rainfall over the central
 767 BoB and less to the north, which is associated with a
 768 southwards shift of the monsoon trough to a more real-
 769 istic location away from the Himalayan foothills. This
 770 change in LPS rainfall again helps explain some of the
 771 changes seen in the mean seasonal rainfall due to cou-
 772 pling. In fact, locally over the BoB the changes in LPS
 773 rainfall account for (almost) all of the changes in the
 774 mean seasonal rainfall, as seen in Fig. 5 (note that val-
 775 ues can exceed 100% due to compounding changes in
 776 mean rainfall from sources other than LPS). However,
 777 the main conclusion is that the effect of increasing res-
 778 olution from 200km to 90km is far greater than that of
 779 air-sea coupling on Indian monsoon LPS.

780 With regards to changes in the effects of coupling
 781 as horizontal resolution is increased, these are much
 782 smaller than the effects of increasing resolution on its
 783 own. Therefore, the differences in effects of coupling
 784 at different resolutions are more than likely largely the
 785 result of the change in atmospheric monsoon base state
 786 between the 200km and 90km resolution simulations.

787 A comparison of the effects of coupling in individual
 788 basins at 90km (N216) horizontal resolution is shown in
 789 Figure 14. In general the number of LPS is substantially
 790 increased in all 90km (N216) experiments shown in Fig-
 791 ure 14 compared to their 200km (N96) equivalents from
 792 Fig. 6. This further highlights that increasing the hori-
 793 zontal resolution from 200km (N96) to 90km (N216)
 794 dominates over the effects of air-sea coupling.

795 The positive effects from resolution and coupling
 796 combined, however, are still not quite as substantial as
 797 the improvements seen when the large-scale monsoon
 798 flow into South Asia is corrected, including the poten-

799 tial effects of precursor disturbances entering the mon-
 800soon region from the Western Pacific, in regional cli-
 801 mate model atmosphere-only experiments (Levine and
 802 Martin, 2018). This suggests the biases in the atmo-
 803 spheric mean state and variability still inhibit the sim-
 804 ulation of monsoon LPS.

3.4.2 Changes to wider area seasonal mean circulation

805 Seasonal means for Jun-Sept of air temperature at 850hPa
 806 and relative humidity at 500hPa are shown in Figure
 807 9. Sufficiently high levels of mid-tropospheric humidity
 808 are considered to be an important factor in the gene-
 809 sis of monsoon LPS (e.g. Sikka 1977). Also, while there
 810 are no large differences in SST between $ATM_{200}[GL]$ /
 811 GL_{200} and $ATM_{90}[GL]$ / GL_{90} (see Fig. 2), differences
 812 in low-level air temperature may be an important fac-
 813 tor in the formation and maintenance of the monsoon
 814 LPS.

815 In general the MetUM simulations are all too dry
 816 over most of India and its surrounding seas, with a
 817 seemingly large influence of dry and hot air from the
 818 continental area to the north west and the Arabian
 819 peninsula (see 850hPa air temperature field), with a
 820 particular lack of moisture availability over Indian land.
 821 There is improvement in available moisture and with
 822 higher resolution over the band covering the Arabian
 823 Sea, India and the Bay of Bengal, although there is still
 824 a remaining dry bias particularly over Indian land. The
 825 low-level air temperature anomalies are improved over
 826 the monsoon trough area at higher resolution. However,
 827 the persistent lack of available moisture over the land
 828 part of the monsoon trough would still act to inhibit
 829 systems from propagating westwards over India within
 830 the monsoon trough.

831 Note that in this case the free-running (atmosphere)
 832 climate model shows the opposite picture to that found
 833 in initialised NWP MetUM simulations by Hunt and
 834 Turner (2017), who find an overestimation of mid-level
 835 moisture availability in the monsoon trough and im-
 836 provements as horizontal resolution is increased, indi-
 837 cating that outside/remote influences likely play a role
 838 in the simulations used in this study rather than simply
 839 being a local convection parametrisation issue.

840 The low-level circulation and precipitation are shown
 841 in Figure 10. Improvements in monsoon rainfall (and
 842 LPS rainfall) over India are also associated with an
 843 improvement to the excessive equatorial Indian Ocean
 844 convection at higher resolution. There are also clear in-
 845 creases in rainfall near bands of sharp (coastal) orogra-
 846 phy, such as the Western Ghats, Himalayas, and along
 847 the Myanmar coast, which are likely a direct result
 848 of the increase in resolution, that will contribute to

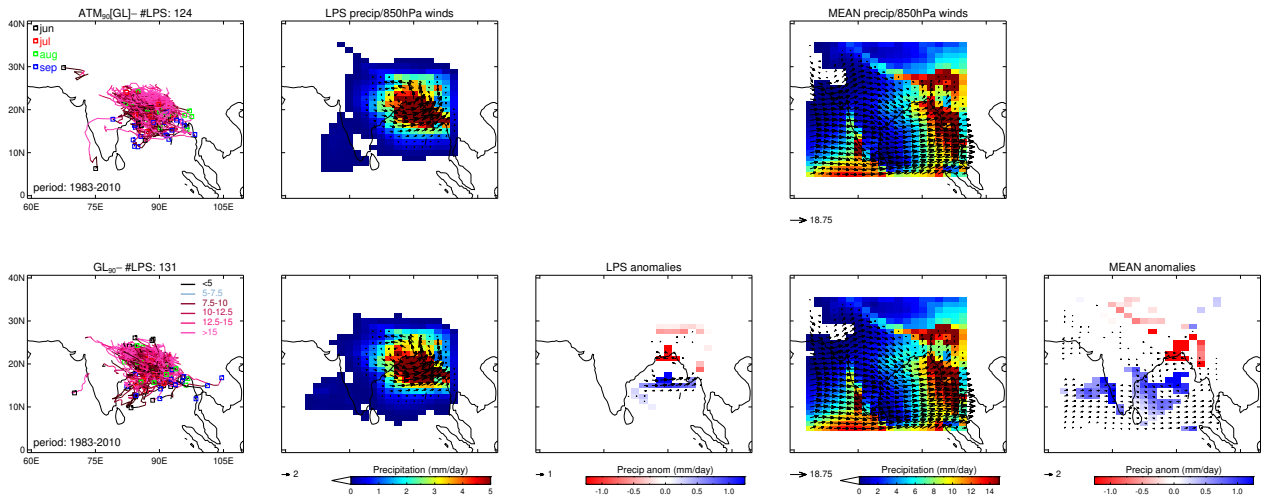


Fig. 8 Monsoon LPS diagnosed in 90km (N216) experiments for 1983-2010 period (only up to 2007 for reanalysis/observations). Top row shows the $ATM_{90}[GL]$ experiment, bottom row shows the GL_{90} experiment, with differences displayed as $[GL_{90} - ATM_{90}[GL]]$. The layout of the plots is as described in Fig. 4.

improved conditions over the Indian region. Furthermore, correcting the inflow conditions into the Indian monsoon zone has been shown to substantially improve monsoon rainfall over India and also monsoon LPS (Levine and Martin 2018), therefore the dampening of equatorial convection may play a role in the improvements to conditions over the Indian region, including the previously discussed changes to moisture availability.

Upper level circulation fields and precipitation are shown in Figure 11. In addition to improvements to convection and upper-level divergence over the equatorial Indian Ocean there are similar improvements to excessive convection over the equatorial Atlantic Ocean with higher resolution. This could contribute to increases in Indian monsoon rainfall (Yadav 2017) and possibly provide favourable conditions for monsoon LPS, although any definite impacts through this route require further investigation. There are also more complex changes across the Pacific, whose impact on the Indian monsoon is unclear and could be investigated.

The effects of air-sea coupling at higher resolution on the upper-level circulation and precipitation are shown in Figure 12. This shows the largest changes in convection due to global coupling ($GL_{90} - ATM_{90}$) over the Indian and Pacific Ocean sectors, while changes over the equatorial Atlantic Ocean are relatively small. There are, however, some changes in the westerly jet across the North Atlantic which may feed into the cyclonic change in upper-level circulation to the north-west of India. If and precisely how this influences monsoon LPS also requires further investigation.

3.4.3 LPS intensity distribution, track and genesis density

Figure 13 shows further statistics for the globally coupled GOML2 experiments compared to their atmosphere-only equivalents. This shows that, once the role of resolution has been eliminated, ERA5 has more occurrences in the moderate intensities compared to all the model simulations, while the model simulations have somewhat more occurrences at higher intensities. This is particularly obvious when looking at the normalised frequency distributions. As well as more low- and moderate strength systems, this also reflects longer-lived strong systems in ERA5, while the systems in the model simulations initially have realistic intensity but are terminated too quickly, with many systems not travelling westwards across India in the monsoon trough.

The result for the 90km (N216) simulation is somewhat similar to analysis by Hunt and Turner (2017, Fig. 12a; note that their 200km (N96) to 90km (N216) jump is more dramatic) of MetUM initialised NWP simulations at different resolutions, although the analysis is slightly different in a number of factors. Firstly, Hunt and Turner (2017) use relative vorticity averaged over a cuboid of 400km surrounding the origin rather than the value at the centre of the tracked system at the 850hPa level as used here. Furthermore, here: the results have been filtered down to T42 resolution; LPS that are weaker than standard definitions for monsoon depressions are included in this study; here we use values at the 850hPa single level instead of an average over 925-750hPa; and perhaps most significantly, the

912 simulations analysed here are free-running (in terms of
 913 atmosphere) climate simulations instead of initialised
 914 NWP simulations.

915 The track density and genesis show far more limited
 916 distributions of LPS in all model simulations compared
 917 to ERA5, with systems concentrated far too much over
 918 the northern Bay of Bengal. They appear to form in
 919 the correct location in the model simulations, but termi-
 920 nate too quickly after making landfall and therefore not
 921 enough systems traverse India westwards in the mon-
 922soon trough. This results in too little contribution to
 923 rainfall over Indian land.

924 *3.4.4 Impact of air-sea coupling in individual basins at
 925 higher resolution*

926 Analysing the impact of the effects of air-sea coupling in
 927 different areas at the higher resolution, the comparison
 928 is made using GL_{90} as the reference simulation. In this
 929 way we examine the contribution to the overall effect
 930 of global coupling from the following four areas:

- 931 **1. Coupling INSIDE Indian Ocean only: $GL_{90} -$
 932 AO_PO_{90} (Fig. 14, second row),**
- 933 **2. Coupling OUTSIDE Indian Ocean: $GL_{90} - IO_{90}$
 934 (Fig. 14, third row),**
- 935 **3. Coupling OUTSIDE Pacific Ocean: $GL_{90} - PO_{90}$
 936 (Fig. 14, fourth row),**
- 937 **4. Coupling OUTSIDE Indian and Pacific Oceans:
 938 $GL_{90} - IO_PO_{90}$ (Fig. 14, fifth row).**

939 The inclusion of air-sea coupling inside the Indian
 940 Ocean ($GL_{90} - AO_PO_{90}$) shows a neutral impact on
 941 LPS numbers, unlike in the equivalent 200km (N96)
 942 simulations. There is though a similar, but smaller, pos-
 943 itive impact on monsoon LPS rainfall over the BoB as
 944 found in the N96 simulations. The differences between
 945 the impacts at the two resolutions is seen clearer in
 946 Figure 15, which shows the $\Delta N216 - \Delta N96$ (90km -
 947 200km) double differences. However, at higher resolu-
 948 tion there is also a small negative impact on monsoon
 949 LPS rainfall over northern India. This perhaps indicates
 950 a role for the negative local effect of air-sea coupling on
 951 LPS strength over the BoB, subsequently weakening
 952 the systems downstream as they move over land. Or
 953 this could be associated with a change in circulation
 954 over India.

955 The inclusion of air-sea coupling outside the Indian
 956 Ocean ($GL_{90} - IO_{90}$) shows a neutral impact both on
 957 LPS numbers and on the mean monsoon flow, again
 958 unlike the equivalent 200km (N96) simulation impact,
 959 while there is a small positive impact on LPS rainfall
 960 over the BoB. The impact on monsoon LPS rainfall is
 961 similar to effects of coupling inside the Indian Ocean

962 ($GL_{90} - AO_PO_{90}$), suggesting again that the effects
 963 of coupling inside and outside the Indian Ocean have a
 964 similar impact on monsoon LPS. However, this impact
 965 is smaller than at 200km (N96) resolution.

966 Of the other areas shown, there is a much clearer
 967 positive effect compared to 200km (N96) on monsoon
 968 LPS rainfall, and consistent effects on the seasonal mean
 969 flow and rainfall, from the coupling outside the In-
 970 dian and Pacific Ocean ($GL_{90} - IO_PO_{90}$), suggest-
 971 ing the Atlantic Ocean coupling has more influence at
 972 higher resolution. There is no obvious direct link be-
 973 tween Atlantic Ocean coupled processes and monsoon
 974 LPS, though indirect links may include downstream
 975 effects of the Atlantic storm-track on the upper-level
 976 westerly flow over the Tibetan Plateau or changes in
 977 the MJO affecting the active/break cycles of the mon-
 978 soon. While the larger-scale circulation changes in the
 979 90km simulations due to global coupling are relatively
 980 small over the Atlantic Ocean (Fig. 12), there are some
 981 changes to the westerly jet across the North Atlantic
 982 which could merit further investigation.

983 The differences in the effects of coupling at the two
 984 different resolutions (Fig. 15) are relatively small for
 985 both coupling outside the Indian Ocean and coupling
 986 outside the Pacific Ocean, although highlight the greater
 987 reduction of mean JJAS Himalayan rainfall at higher
 988 resolution, which is part of the southwards shift of mean
 989 JJAS rainfall from the Himalayas seen at both resolu-
 990 tions. The last row of Fig. 15 highlights the increased
 991 LPS and mean rainfall at higher resolution with cou-
 992pling outside the Indian and Pacific Ocean.

4 Discussion and Conclusions

993 The effects of air-sea coupling and horizontal resolu-
 994 tion on the climate model simulation of monsoon LPS,
 995 which are important contributors to (extreme) Indian
 996 monsoon rainfall (Sikka 1977; Krishnamurthy and Ajayam-
 997 han 2010; Praveen et al. 2015; Hunt et al. 2016), are
 998 examined in order to understand the poor representa-
 999 tion of LPS in current global climate models (Ashok
 1000 et al. 2000; Sabre et al. 2000; Stowasser et al. 2009;
 1001 Praveen et al. 2015, Levine and Martin 2018). While
 1002 increasing horizontal resolution may be beneficial for
 1003 capturing more detail, understanding the (combined)
 1004 effects of air-sea coupling and horizontal resolution us-
 1005 ing current coupled models is hampered by the pres-
 1006 ence of widespread tropical SST biases. Therefore, in
 1007 this study, we use climate simulations from MetUM-
 1008 GOML2. This model couples the MetUM GA6 atmo-
 1009 sphere to a mixed-layer ocean, which constrains the
 1010 SSTs to observations, thereby minimising (but not eli-
 1011 minating) the effects of SST biases that are common in

many fully coupled atmosphere-ocean models. The robustness of the remaining SST biases between atmosphere-only MetUM-GOML2 simulations at different resolutions is evidence that this experimental approach ensures a consistent ocean mean state between resolutions, so that differences between the simulations can be attributed to differences in resolution only. Furthermore, while the atmospheric monsoon base state may be slightly different from the standard fully coupled and AMIP-style MetUM simulations, the isolated comparison of MetUM-GOML2 mixed-layer ocean coupled simulations and their equivalent atmosphere-only simulations (forced with GOML2 SSTs) does provide a cleaner decomposition into effects from coupling and from resolution.

Global coupling in the MetUM-GOML2 simulations ($GL - ATM[GL]$), when SST biases are excluded, has a neutral impact on the number of LPS formed, while the associated rainfall is somewhat reduced due to a negative air-sea feedback reducing the strength of atmospheric convection and weakening individual LPS, consistent with dampening effects on extreme tropical rainfall found by Hiron et al. (2018). When compared with a standard MetUM AMIP-type uncoupled run forced with observed SSTs, the MetUM-GOML2 global coupling results in larger numbers of LPS and associated rainfall, suggesting that the SST biases in MetUM-GOML2, though small, do play a role in altering the mean state of the monsoon. While this does not affect the MetUM-GOML2 global coupling ($GL - ATM[GL]$) comparison, it is relevant in the comparison of regionally coupled simulations, due to differences in SST in the uncoupled regions. This is due to differences in interannual SST variability, for example the uncoupled regions in MetUM-GOML2 coupled simulations are prescribed with climatological monthly-varying observed SST, and do not contain interannual variability. Furthermore, comparing coupled with uncoupled regions in the MetUM2-GOML2 regionally coupled simulations is affected by the remaining SST biases developing in the coupled regions.

It is found that the regional simulations are particularly sensitive to localised coupling in the Indian and Pacific Oceans, which also has a positive effect on both the number of LPS and associated rainfall when compared with an uncoupled run forced with time-varying observed SSTs. As well as the direct effects of air-sea coupling in the individual oceans, this may also involve the aforementioned differences in SST, and in this case it seems likely that SST biases are at least partly responsible for the positive effects from Indian and Pacific Ocean coupling.

The remote effect of coupling within the Pacific Ocean may involve impacts on the Indian monsoon through the Walker circulation, or perhaps a change in the prevalence of westwards-travelling pre-cursor disturbances, which are thought to originate in the Western Pacific (Saha et al. 1981). These mechanisms have been suggested to affect the representation of monsoon LPS in regional climate model simulations (Levine and Martin, 2018). At higher resolution there is also an increased effect on LPS from coupling over the Atlantic Ocean. Further work is needed to properly establish the nature of these remote effects, which could also be the result of noise as only a single ensemble member is used in this study.

While global air-sea coupling, in the absence of SST biases, is shown to have a relatively small impact, it is found that increasing the horizontal resolution from N96 (200km) to N216 (90km) results in substantially larger improvements to both the simulation of Indian monsoon LPS and the mean state monsoon. Although the positive differences here are smaller than the benefits of eliminating remote biases, such as excessive equatorial Indian Ocean convection, observed in regional (atmosphere-only) climate model simulations (Levine and Martin, 2018), the effects of increasing resolution on LPS are found to be larger than in previous configurations of the MetUM (Johnson et al. 2016). While there are increased LPS numbers forming over the Bay of Bengal and increased LPS rainfall over north-eastern India in the higher resolution MetUM-GOML2 simulations, it is still found that the systems decay too soon after making landfall over India and many fail to continue westwards across India within the monsoon trough. This is consistent with the anomalously hot and dry conditions that prevail over Indian land and make for unfavourable conditions for LPS to be formed or maintained.

There are several factors that likely contribute to the improvements in LPS with increased horizontal resolution, including improved resolving of the structure of the LPS. This effect was seen using initialised NWP simulations of monsoon depressions using the same GA6 MetUM configuration by Hunt and Turner (2017), who found the greatest improvements when moving from N96 (denoted in this paper as 200km) to N216 (denoted in this paper as 90km), with little improvement beyond that. Improvements to the larger-scale circulation at higher resolution are also likely important, with Levine and Martin (2018) showing that improving the wider region circulation can have huge benefits to the representation of LPS. As discussed in previous sections, this probably relates to various factors, including dampening of excessive convection over the equatorial Indian

Ocean and changes to representation of orography, the latter of which is evident in rainfall changes near bands of sharp (coastal) mountains, and will contribute to improved conditions over the Indian region. Furthermore, there are possible improvements to pre-cursor disturbances from the W Pacific (Levine and Martin, 2018) that are sometimes linked to W Pacific typhoons or tropical storms making landfall (Saha et al 1981). This latter process may play a more prominent role at higher resolution due to improvements to tropical cyclone frequency and structure (Roberts et al. 2020). The new dynamical core ENDGAME included in the MetUM GA6 configuration used in this study enhances tropical variability, including tropical cyclone activity (Walters et al. 2017), and may play a role in the larger changes seen to the monsoon circulation with increased horizontal resolution compared to previous configurations (Johnson et al. 2016).

It is important to note that the methodology used in this study has some limitations, some of which are described in more detail in Hiron et al. (2015) and Peatman and Klingaman (2018): 1) The experiments are relatively short at approximately 30 years. While other studies using this GOML2 methodology (e.g. Peatman and Klingaman (2018)) have used simulations of similar length and found robust results for changes in seasonal mean and intraseasonal precipitation, longer simulations may confirm the findings presented here. 2) While the experiments using the MetUM-GOML2 framework allow a relatively pure comparison of effects of air-sea coupling and resolution, the atmospheric base state is a little different to the standard MetUM AMIP-style simulations, mainly due to remaining cold SST biases (which are still relatively small compared to the fully coupled MetUM), the effects of which require further investigation. 3) In terms of the coupling, the lack of ocean dynamics in the MetUM-GOML2 model means there is no representation of ENSO or IOD variability in the ocean (Hiron et al. 2015). This may be important if there are non-linear effects of ENSO and IOD variability on the number of LPS and their associated rainfall. 4) The uncoupled regions of the regionally coupled simulation are forced with climatological monthly-varying observed SST, which introduces differences in interannual SST variability compared to the globally coupled simulation and the atmosphere-only (AMIP-type) simulation forced with time-varying observed SST. Furthermore, the uncoupled regions do not include any SST biases or interannual variability present in those regions in the atmosphere-only simulation forced with SSTs from the globally coupled simulation. 5) The current study has only tested two horizontal resolutions. 6) The MetUM atmosphere model used has an inherent

strong mean dry bias in Indian monsoon rainfall (part of which involves the lack of LPS and associated rainfall, which is also associated with the limited westwards progression over Indian land of these systems).

It is possible that all these factors may influence the results. For example, the positive effects from resolution and coupling combined are still not quite as substantial as the improvements seen when the large-scale monsoon flow into South Asia is corrected (Levine and Martin, 2018), which suggests that the inherent MetUM biases in the atmospheric mean state and variability still inhibit the simulation of monsoon LPS. Using other models that have different mean biases and/or moving to higher horizontal resolutions than used here (< 90km) may show different sensitivities, although it is worth noting that Hunt and Turner (2017) found little improvements in MetUM NWP case studies of monsoon depressions when resolution was increased beyond 63-39km. The limitations discussed here require further attention in subsequent investigations.

Acknowledgements This work and its contributors (Richard Levine and Gill Martin) was supported through the Weather and Climate Science for Service Partnership (WCSSP) India, a collaborative initiative between the Met Office, supported by the UK Government's Newton Fund, and the Indian Ministry of Earth Sciences (MoES). Nicholas Klingaman was supported by an Independent Research Fellowship from the Natural Environment Research Council (NE/L010976/1) and by the NERC/Global Challenges Research Fund programme Atmospheric hazards in developing countries: risk assessment and early warnings (ACREW). Simon Peatman was supported by the NERC Bay of Bengal Boundary Layer Experiment project of the (NE/L013800/1). ERA5 figures in this paper have been generated using Copernicus Climate Change Service Information 2020. The authors would like to thank the two anonymous reviewers for suggestions that helped improve the manuscript.

References

1. Adler RF, Huffman GJ, Chang A, Ferraro R, Xie PP, Janowiak J, Rudolf B, Schneider U, Curtis S, Bolvin D, Gruber A, Susskind J, Arkin P, Nelkin E (2003). The version-2 global precipitation climatology project (GPCP) monthly precipitation analysis (1979–present). *J Clim* 4:1147–1167
2. Ashok K, Soman MK, Satyan V (2000). Simulation of monsoon disturbances in a GCM. *Pure Appl Geophys* 157:1509–1539. 2000
3. Bollasina M and Nigam S (2009). Indian Ocean SST, evaporation, and precipitation during the South Asian summer monsoon in IPCC-AR4 coupled simulations. *Clim Dyn* 33: 1017. <https://doi.org/10.1007/s00382-008-0477-4>
4. Bollasina MA, Ming Y (2013). The general circulation model precipitation bias over the southwestern equatorial Indian Ocean and its implications for simulating the South Asian monsoon. *Clim Dyn* 40: 823–838. <https://doi.org/10.1007/s00382-012-1347-7>

1227 5. Copernicus Climate Change Service (C3S) (2017):
1228 ERA5: Fifth generation of ECMWF atmospheric re-
1229 analyses of the global climate. Copernicus Climate
1230 Change Service Climate Data Store (CDS), 2020.
1231 <https://cds.climate.copernicus.eu/cdsapp#!/home>

1232 6. DeMott CA, Stan C, Randall DA, Branson MD (2014).
1233 Intraseasonal variability in coupled GCMs: The roles of
1234 ocean feedbacks and model physics. *J Clim* 27: 4970–4995.
1235 <https://doi.org/10.1175/JCLI-D-13-00760.1>

1236 7. DeMott CA, Klingaman NP, Woolnough SJ (2015).
1237 Atmosphere–Ocean Coupled Processes in the Madden–
1238 Julian Oscillation. *Rev Geophys* 53: 1099–1154.
1239 <https://doi.org/10.1002/2014RG000478>

1240 8. Fu X and Wang B (2004). Differences of boreal sum-
1241 mer intraseasonal oscillations simulated in an atmos-
1242 phere–ocean coupled model and an atmosphere-only model.
1243 *J Clim* 17: 1263–1271. [https://doi.org/10.1175/1520-0442\(2004\)017<1263:DOBSIO>2.0.CO;2](https://doi.org/10.1175/1520-0442(2004)017<1263:DOBSIO>2.0.CO;2)

1244 9. Gao Y, Klingaman NP, DeMott CA, Hsu P-C (2019). Diagnosing ocean feedbacks to the BSISO: SST-
1245 modulated surface fluxes and the moist static en-
1246 ergy budget. *J Geophys Res Atmos* 124: 146–170.
1247 <https://doi.org/10.1029/2018JD029303>

1248 10. Gates WL et al. (1998). An Overview of the Results of
1249 the Atmospheric Model Intercomparison Project (AMIP I). *Bull Amer Meteor Soc* 73: 1962–1970.

1250 11. Halkides DJ, Waliser DE, Lee T, Menemenlis D, Guan
1251 B (2015). Quantifying the processes controlling intraseasonal
1252 mixed-layer temperature variability in the tropical
1253 Indian Ocean. *J Geophys Res Oceans* 120: 692–715.
1254 <https://doi.org/10.1002/2014JC010139>

1255 12. Hiron LC, Klingaman NP, Woolnough SJ (2015), MetUM-GOML1: a near-globally coupled
1256 atmosphere–ocean-mixed-layer model, *Geosci Model Dev*
1257 8: 363–379, 2015. <https://doi.org/10.5194/gmd-8-363-2015>

1258 13. Hiron LC, Klingaman NP, Woolnough SJ (2018). The
1259 impact of air-sea interactions on the representation of trop-
1260 ical precipitation extremes. *J Adv Model Earth Sy* 10:
1261 550–559. <https://doi.org/10.1002/2017MS001252>

1262 14. Hodges KI (1994). A general method for tracking analysis
1263 and its application to meteorological data. *Mon Weather
1264 Rev* 122:2573–2586

1265 15. Hsu W-C, Patricola M, Chang P (2019). The im-
1266 pact of climate model sea surface temperature biases on
1267 tropical cyclone simulations. *Clim Dyn* 53(1–2): 173–192.
1268 <https://doi.org/10.1007/s00382-018-4577-5>

1269 16. Hunt KMR, Turner AG, Inness PM, Parker DE, Levine
1270 RC (2016). On the structure and dynamics of Indian mon-
1271soon depressions. *Mon Weather Rev* 144(9): 3391–3416.
1272 <https://doi.org/10.1175/MWR-D-15-0138.1>

1273 17. Hunt KMR and Turner AG (2017). The effect of
1274 horizontal resolution on Indian monsoon depressions in
1275 the Met Office NWP model. *Q J R Meteorol Soc*
1276 <https://doi.org/10.1002/qj.3030>

1277 18. Johnson SJ, Levine RC, Turner AG, Martin GM, Wool-
1278 nough SJ, Schiemann R, Mizieliński MS, Roberts MJ, Vi-
1279 dale PL, Demory M-E, Strachan J (2016). The resolution
1280 sensitivity of the South Asian Monsoon and Indo-Pacific
1281 in a global 0.35 degree AGCM. *Clim Dynam.* 46: 807.
1282 <https://doi.org/10.1007/s00382-015-2614-1>

1283 19. Karmacharya J, Levine RC, Jones R, Moufouma-Okia
1284 W, New M (2015). Sensitivity of systematic biases in
1285 South Asian summer monsoon simulations to regional cli-
1286 mate model domain size and implications for downscaled
1287 regional process studies. *Clim Dynam.* 45(1–2):213–231.
1288 <https://doi.org/10.1007/s00382-015-2565-6>

1289 20. Karmacharya J, New M, Jones R, Levine R (2016).
1290 Added value of a high resolution regional climate
1291 model in simulation of intraseasonal variability of
1292 the South Asian summer monsoon. *Int J Climatol.*
1293 <https://doi.org/10.1002/joc.4767>

1294 21. Klingaman NP and Woolnough SJ (2014). The role of
1295 air-sea coupling in the simulation of the Madden-Julian os-
1296 cillation in the Hadley Centre model. *Q J Roy Meteor Soc*
1297 140:2272–2286. <https://doi.org/10.1002/qj.2295>

1298 22. Krishnamurthy V and Shukla J (2007). Intraseasonal and
1299 seasonally persisting patterns of Indian monsoon rainfall. *J
1300 Clim* 20:3–20. <https://doi.org/10.1175/JCLI3981.1>

1301 23. Krishnamurthy V and Ajayamohan RS (2010). Com-
1302 posite Structure of Monsoon Low Pressure Systems and
1303 Its Relation to Indian Rainfall. *J Clim.* 23:4285–4305.
1304 <https://doi.org/10.1175/2010JCLI2953.1>

1305 24. Levine RC and Martin GM (2018). On the cli-
1306 mate model simulation of Indian monsoon low pres-
1307 sure systems and the effect of remote disturbances
1308 and systematic biases. *Clim Dynam* 50(11–12):4721–4743.
1309 <https://doi.org/10.1007/s00382-017-3900-x>

1310 25. Levine RC, Turner AG, Marathayil D, Martin GM
1311 (2013). The role of northern Arabian Sea surface temper-
1312 ature biases in CMIP5 model simulations and future pro-
1313 jections of Indian summer monsoon rainfall. *Clim Dyn* 41:
1314 155–172. <https://doi.org/10.1007/s00382-012-1656-x>

1315 26. Levine RC, Turner AG (2012). Dependence of In-
1316 dian monsoon rainfall on moisture fluxes across the
1317 AS and the impact of coupled model sea surface
1318 temperature biases. *Clim Dynam* 38(11–12):2167–2190.
1319 <https://doi.org/10.1007/s00382-011-1096-z>

1320 27. Peatman SC and Klingaman NP (2018). The Indian
1321 summer monsoon in MetUM-GOML2.0: effects of air–sea
1322 coupling and resolution. *Geosci Model Dev* 11:4693–4709.
1323 <https://doi.org/10.5194/gmd-11-4693-2018>

1324 28. Praveen V, Sandeep S, Ajayamohan RS (2015). On
1325 the Relationship between Mean Monsoon Precipitation
1326 and Low Pressure Systems in Climate Model Simulations.
1327 *J Clim* 28:5305–5324. <https://doi.org/10.1175/JCLI-D-14-00415.1>

1328 29. Prodhomme C, Terray P, Masson S et al. (2014). Impacts
1329 of Indian Ocean SST biases on the Indian Monsoon: as sim-
1330 ulated in a global coupled model. *Clim Dyn* 42: 271–290.
1331 <https://doi.org/10.1007/s00382-013-1671-6>

1332 30. Reynolds RW, Smith TM, Liu C, Chelton DB, Casey
1333 KS, Schlax MG (2007) Daily high-resolution-blended anal-
1334 yses for sea surface temperature. *J Clim* 20:5473–5496.
1335 <https://doi.org/10.1175/2007JCLI1824.1>

1336 31. Roberts MJ et al. (2020). Impact of Model Resolu-
1337 tion on Tropical Cyclone Simulation Using the High-
1338 ResMIP–PRIMAVERA Multimodel Ensemble. *J Clim* 33:
1339 2557–2583. <https://doi.org/10.1175/JCLI-D-19-0639.1>

1340 32. Sabre M, Hodges KI, Laval K, Polcher J, Desalmand F
1341 (2000). Simulation of monsoon disturbances in the LMD
1342 GCM. *Mon Weather Rev* 128:3752–3771

1343 33. Saha K, Sanders F, Shukla J (1981). Westward
1344 Propagating Predecessors of Monsoon Depressions, *Mon
1345 Weather Rev.* 109:330–343. [https://doi.org/10.1175/1520-0493\(1981\)109<0330:WPPOMD>2.0.CO;2](https://doi.org/10.1175/1520-0493(1981)109<0330:WPPOMD>2.0.CO;2)

1346 34. Shukla RP, Huang B (2016). Interannual variability of
1347 the Indian summer monsoon associated with the air–sea
1348 feedback in the northern Indian Ocean. *Clim Dyn* 46:
1349 1977–1990. <https://doi.org/10.1007/s00382-015-2687-x>

1350 35. Sikka DR (1977). Some aspects of the life history, struc-
1351 ture and movement of monsoon depressions. *Pure Appl
1352 Geophys.* 115:1501–1529

1359 36. Smith DM, Murphy JM (2007). An objective ocean tem-
1360 perature and salinity analysis using covariances from a
1361 global climate model. *J Geophys Res Ocean* 112 (C02022).
1362 <https://doi.org/10.1029/2005JC003172>

1363 37. Stowasser M, Annamalai H, Hafner J (2009). Response
1364 of the South Asian summer monsoon to global warm-
1365 ing: mean and synoptic systems. *J Clim* 22:1014–1036.
1366 <https://doi.org/10.1175/2008JCLI2218.1>

1367 38. Subrahmanyam B, Murty VSN, Sharp RJ, O'Brien
1368 JJ (2005). Air-sea Coupling During the Tropical Cy-
1369 clones in the Indian Ocean: A Case Study Using Satel-
1370 lite Observations. *Pure appl geophys* 162: 1643-1672.
1371 <https://doi.org/10.1007/s00024-005-2687-6>

1372 39. Wainwright CM, Hiron LC, Klingaman NP, Allan RP,
1373 Black E, Turner AG (2019) The impact of air-sea cou-
1374 pling and ocean biases on the seasonal cycle of south-
1375 ern West African precipitation. *Clim Dyn* 53: 7027–7044.
1376 <https://doi.org/10.1007/s00382-019-04973-0>

1377 40. Walters DN et al. (2011). The Met Office Unified
1378 Model Global Atmosphere 6.0/6.1 and JULES Global
1379 Land 3.0/3.1 configurations. *Geosci Model Dev* 4: 919–941.
1380 <https://doi.org/10.5194/gmd-4-919-2011>

1381 41. Walters DN et al. (2017). The Met Office Unified
1382 Model Global Atmosphere 6.0/6.1 and JULES Global Land
1383 6.0/6.1 configurations. *Geosci Model Dev* 10(4), 1487-1520.
1384 <https://doi.org/10.5194/gmd-10-1487-2017>

1385 42. Williams KD et al. (2015). The Met Office Global Cou-
1386 pled model 2.0 (GC2) configuration. *Geosci Model Dev* 8:
1387 1509–1524. <https://doi.org/10.5194/gmd-8-1509-2015>

1388 43. Wu G, Guan Y, Liu Y, Yan J, Mao J (2012). Air-sea
1389 interaction and formation of the Asian summer monsoon
1390 onset vortex over the Bay of Bengal. *Clim Dyn* 38(1-2):
1391 261-279. <https://doi.org/10.1007/s00382-010-0978-9>

1392 44. Yadav RK (2017). On the relationship between east
1393 equatorial Atlantic SST and ISM through Eurasian wave.
1394 *Clim Dyn* 48: 281–295. <https://doi.org/10.1007/s00382-016-3074-y>

1395 45. Yatagai A, Kamiguchi K, Arakawa O, Hamada A, Ya-
1396 sutomi N, Kitoh A (2012). APHRODITE: Constructing a
1397 Long-Term Daily Gridded Precipitation Dataset for Asia
1398 Based on a Dense Network of Rain Gauges. *BAMS*. Septem-
1399 ber 2012:1401-1415

1400

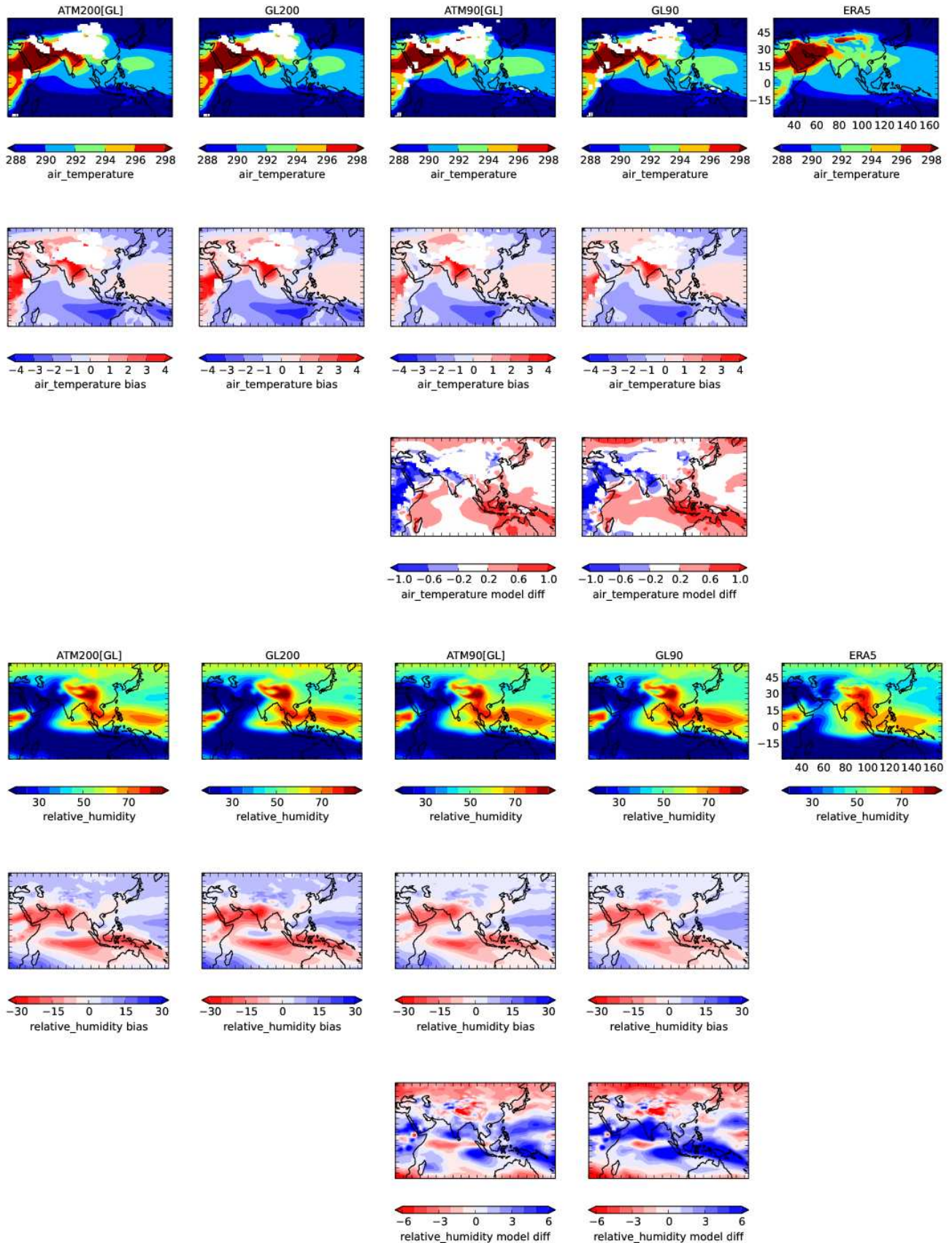


Fig. 9 Row (1) Air temperature (in K, average for Jun-Sept) at 850hPa. Row (2) Differences compared to ERA5. Row (3) 90km minus 200km ($ATM_{90}[GL] - ATM_{200}[GL]$ and $GL_{90} - GL_{200}$) and relative humidity (in %, average for Jun-Sept) at 500hPa for Jun-Sept and differences compared to ERA5 in same layout as for air temperature. Seasonal Jun-Sept means for the period 1983-2010. The ERA5 figures have been generated using Copernicus Climate Change Service Information 2020.

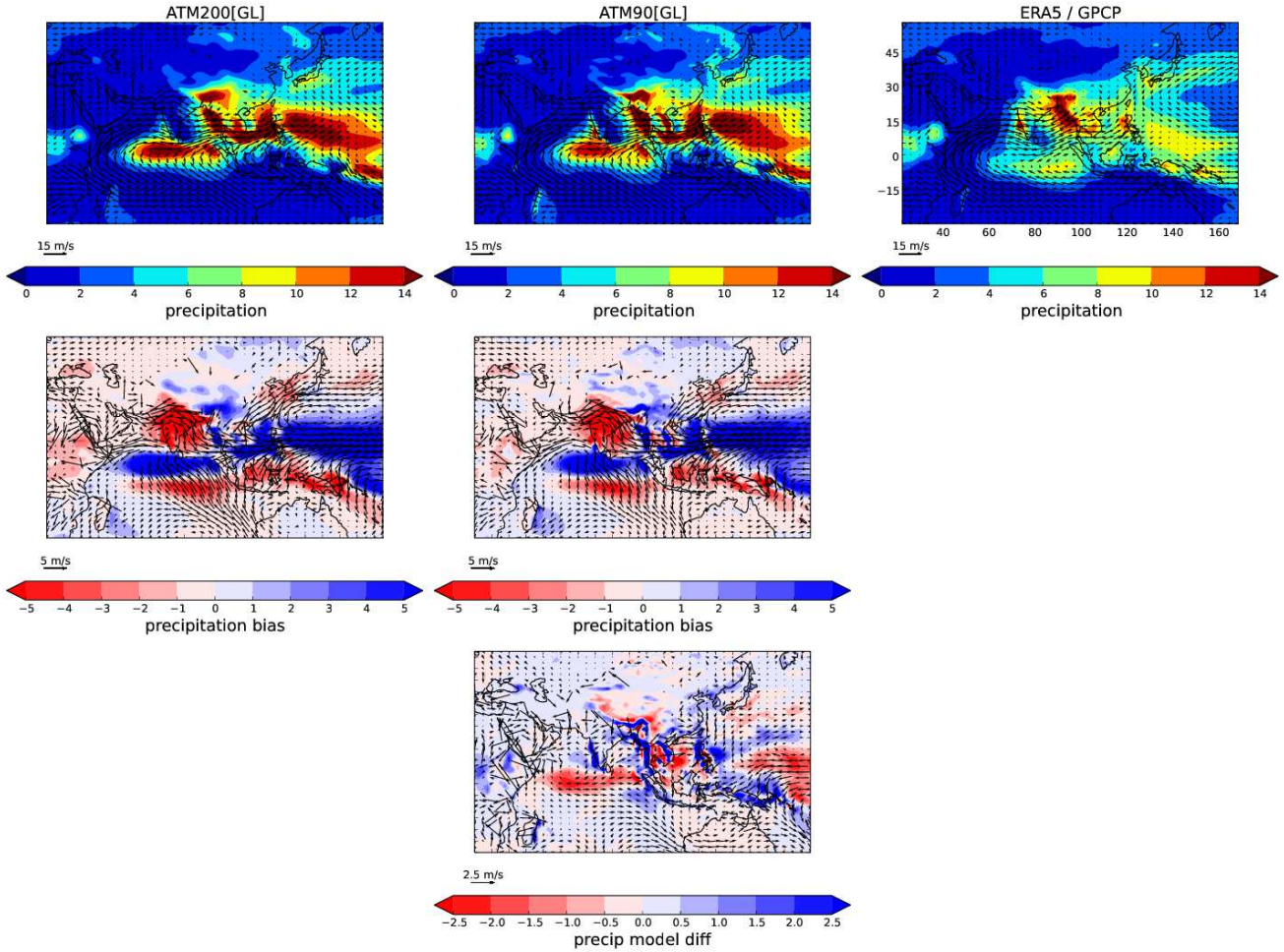


Fig. 10 Row (1) Precipitation (mm/day, coloured contours) and 850hPa winds (m/s, vectors). Row (2) Differences compared to ERA5 and GPCP precipitation. Row (3) 90km minus 200km ($ATM_{90}[GL] - ATM_{200}[GL]$). Seasonal Jun-Sept means for the period 1983-2010. The ERA5 figures have been generated using Copernicus Climate Change Service Information 2020.

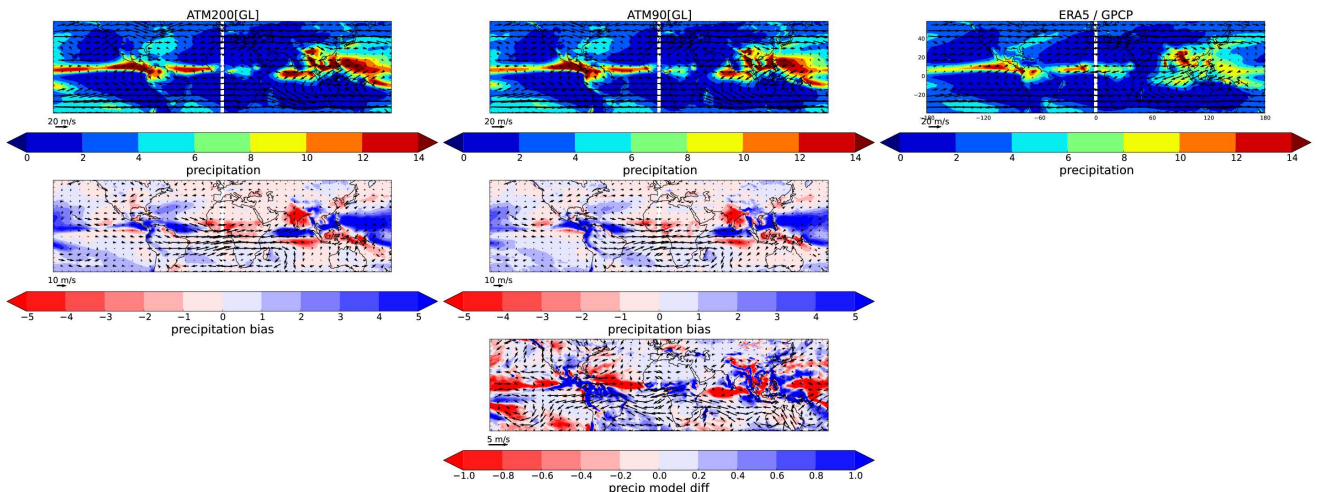


Fig. 11 Row (1) Precipitation (mm/day, coloured contours) and 200hPa winds (m/s, vectors). Row (2) Differences compared to ERA5 and GPCP precipitation. Row (3) 90km minus 200km ($ATM_{90}[GL] - ATM_{200}[GL]$). Seasonal Jun-Sept means for the period 1983-2010. The ERA5 figures have been generated using Copernicus Climate Change Service Information 2020.

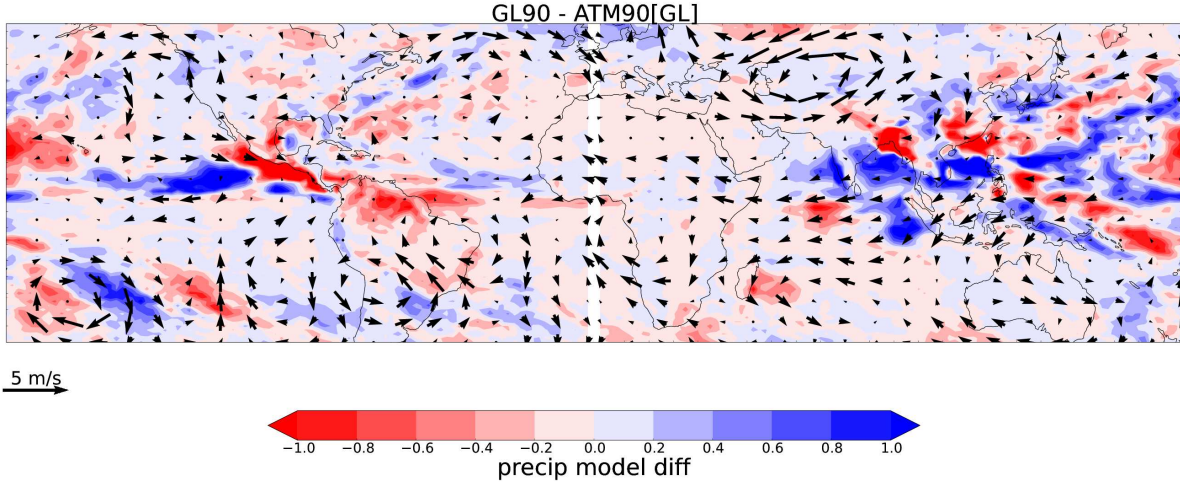


Fig. 12 Differences in precipitation (mm/day, coloured contours) and 200hPa winds (m/s, vectors) for global coupling minus atmosphere-only simulations at 90km ($GL_{90}[GL]$ – $ATM_{90}[GL]$). Seasonal Jun-Sept mean for the period 1983–2010.

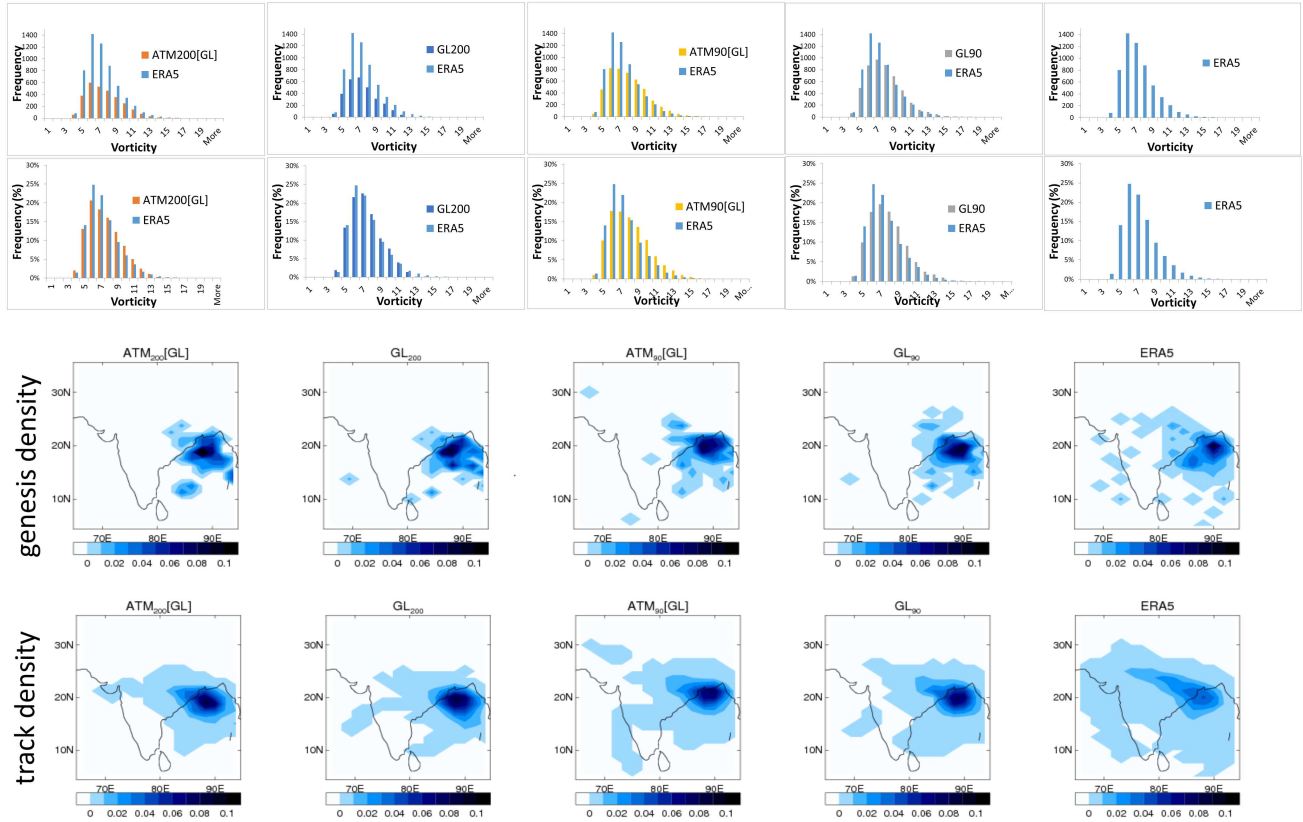


Fig. 13 LPS intensity histograms (as described in Fig. 1). First row is total occurrences, second row is normalised frequency distribution, third row is LPS track genesis (from equation 2), fourth row is LPS track density (from equation 1). The columns show experiments $ATM_{200}[GL]$, GL_{200} , $ATM_{90}[GL]$, GL_{90} , $ERA5$. The ERA5 figures have been generated using Copernicus Climate Change Service Information 2020.

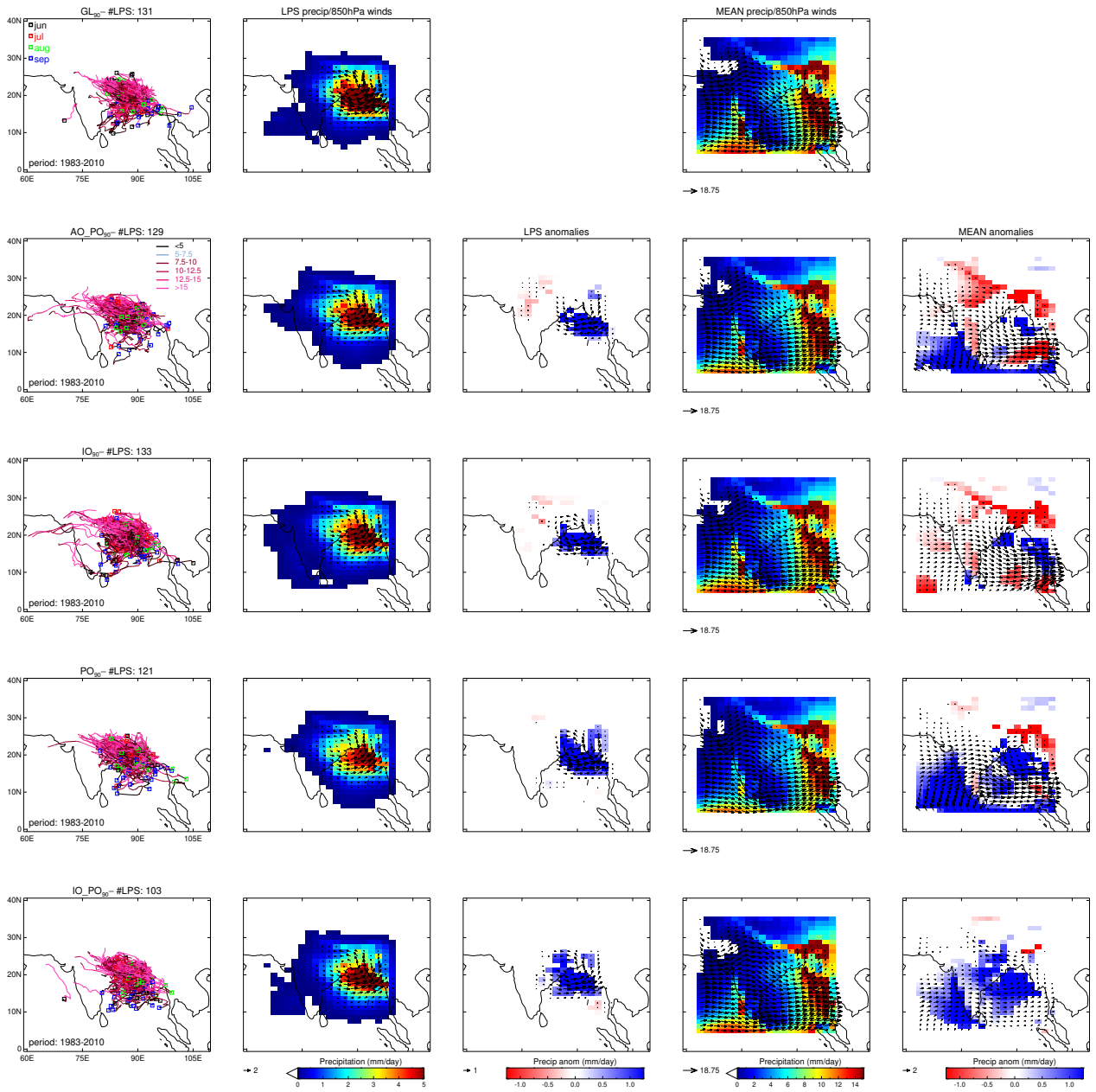


Fig. 14 Coupling sensitivity of 90km (N216) simulations for 1983-2010 period. Top row shows the Global Coupling (obs) experiment, while subsequent rows show the results for regional coupling and differences displayed as [GL₉₀ - AO_{PO}₉₀] (coupling INSIDE Indian Ocean), [GL₉₀ - IO₉₀] (coupling OUTSIDE Indian Ocean), [GL₉₀ - PO₉₀] (coupling OUTSIDE Pacific Ocean), [GL₉₀ - IO_{PO}₉₀] (coupling OUTSIDE Indian and Pacific Oceans). The layout of the plots is as described in Fig. 4.

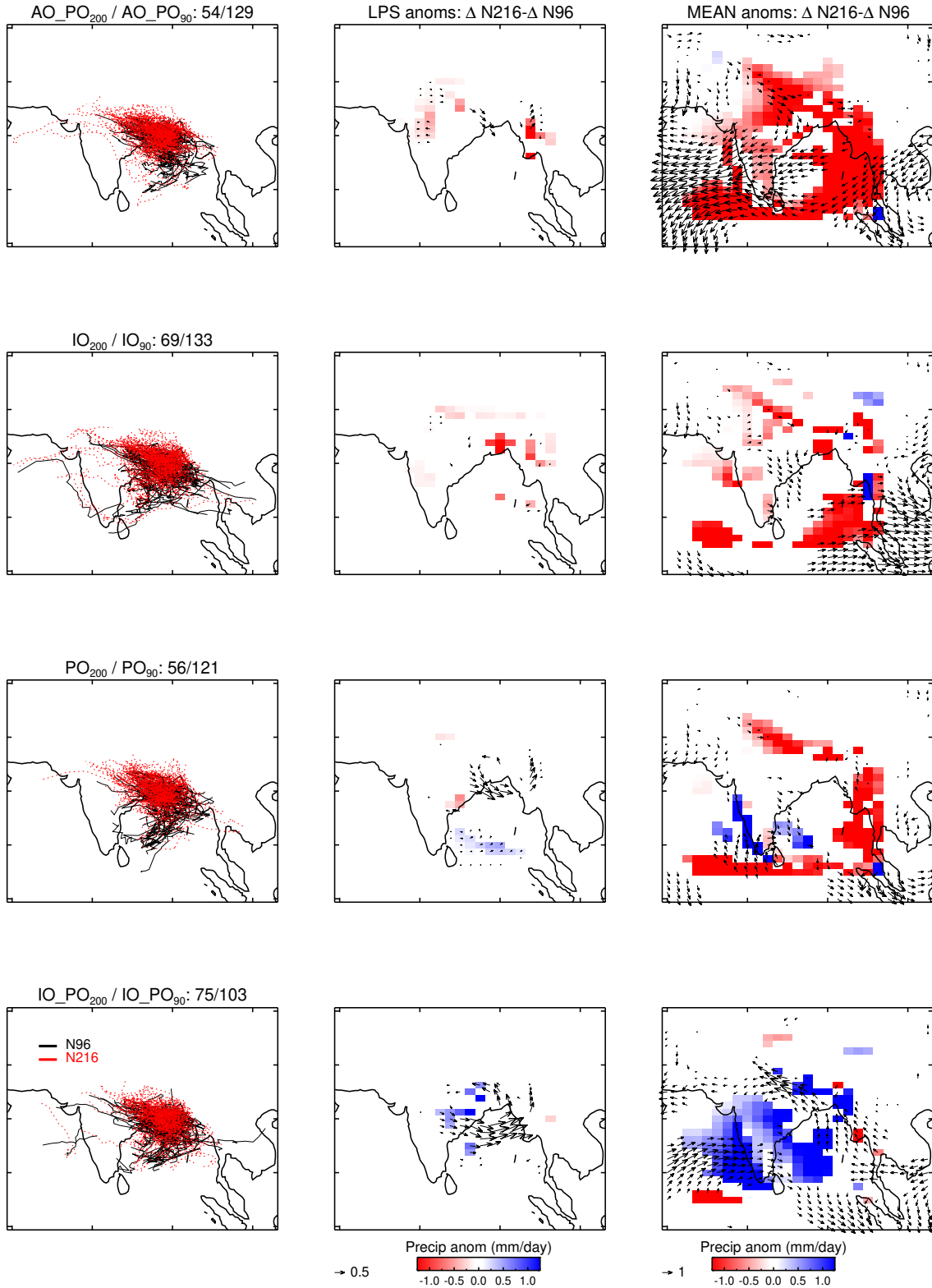


Fig. 15 Comparison of coupling sensitivity for coupling experiments (EXPT) at 90km (N216) versus 200km (N96) simulations for 1983-2010 period in terms of double differences: $\Delta N216 - \Delta N96 = (GL_{90} - EXPT_{90}) - (GL_{200} - EXPT_{200})$. The *first panel on left hand-side* shows LPS trajectories with the total number of LPS in title for N96 (black) and N216 (red dotted). The *second panel from left* shows double differences in LPS contribution to Jun-Sept seasonal mean precipitation (mm/day) and 850hPa winds (m/s, black vectors). The *third panel from left* shows double differences Jun-Sept seasonal mean precipitation (mm/day) and 850hPa wind (m/s) contributions. All data in panels two and three are plotted on a common 200km (N96; $1.875^\circ \times 1.25^\circ$) grid. Only significant differences and vectors at 90% level using a student t-test are shown. Values exceeding the colour scale maxima are capped at the relevant maximum colour value.